UNIVERSITY OF CALIFORNIA, SAN DIEGO

**Trace element abundances and Sr-Nd-Pb isotopic constraints on the petrogenesis of Juan Fernandez lavas**

A thesis submitted in partial satisfaction of the
requirements for the degree
Master of Science

in

Earth Sciences

by

Thi Bich Truong

Committee in charge:

Professor Paterno Castillo, Chair
Professor James Day
Professor David Hilton

2015

The Thesis of Thi Bich Truong is approved, and it is acceptable in quality and form for publication on microfilm and electronically:

---

---

---

Chair

University of California, San Diego

2015

# DEDICATION

Dedicated to my parents Thuy Nguyen and Hung Truong.

# EPIGRAPH

There is no good way to comprehend any one aspect of geology without studying the wider matrix in which it rests.

*John McPhee*

TABLE OF CONTENTS

LIST OF FIGURES

LIST OF TABLES

ACKNOWLEDGEMENTS

I would like to thank, first and foremost, my advisor for this project, Professor Paterno Castillo for his constant availability and encouragement through 4 years of work. Thank you to my committee members, James Day and David Hilton for offering their expertise time and time again for my own benefit.

Thanks to everyone at SIO who made this research possible: Joshua Reeves with my degree requirements, and Chris MacIsaac for the guidance in the lab, and especially for saving my first strontium cut in the TIMS when it grew legs. Thank you to Lisa Tauxe for the suggestion in programming class that we should learn LaTeX. I am also grateful for the help of UCSD librarians who were able to elucidate the nuances of accessing obscure articles.

ABSTRACT OF THE THESIS

**Trace element abundances and Sr-Nd-Pb isotopic constraints on the petrogenesis of Juan Fernandez lavas**

by

Thi Bich Truong

Master of Science in Earth Sciences

University of California, San Diego, 2015

Professor Paterno Castillo, Chair

The origin of the Juan Fernandez Islands in the South Pacific is of geologic importance due to high-$^{3}He/^{4}He$ ratios that span a considerable range (7.8-18.0 $R_A$). To constrain the petrogenesis and mantle source of the islands, bulk trace element abundances and Pb isotopic compositions were obtained for mafic lavas from islands Robinson Crusoe and Alexander Selkirk. Trace element data confirm grouping where on Robinson Crusoe, group I represents the shield-building phase and group II represents post-shield building. Group III represents shield-building on Alexander Selkirk. Sub-parallel incompatible trace elements patterns among all

samples suggest a common mantle origin. Shield-building groups I and III have nearly identical trace element concentrations, and lower Nb/Zr, Ba/Zr and $La/Yb_N$ than the more enriched group II. Incompatible trace element modeling indicate group III was produced by the highest degree of partial melting, while low degrees of partial melting plus fractional crystallization account for group II. Robinson Crusoe lavas exhibit more radiogenic Pb isotopes ($^{206}Pb/^{204}Pb$: 19.163-19.292) than Alexander Selkirk ($^{206}Pb/^{204}Pb$: 18.939-19.228). The range of Sr-Nd-Pb and He isotopes result from variable degrees of partial melting of a slightly heterogeneous mantle plume source. The source contains an EM1 mantle component, and lies near the focus zone (FOZO). Group I represent young HIMU in the source of ocean island basalts while group III represent EM1. Juan Fernandez is unlike other high-$^3He/^4He$ volcanic chains for lack of binary mixing between its low and high-$^3He/^4He$ sources, showing no correlation between Sr-Nd-Pb and He isotopes.

# 1 Introduction

Mid-ocean ridge basalts (MORB) are characterized by a more predictable and homogeneous composition than other oceanic basaltic lavas. They are primarily tholeiitic basalts, depleted in highly incompatible relative to less incompatible elements and encompass a relatively narrow range of long-lived radiogenic isotopic compositions [*Hofmann*, 2003, and references therein]. Their distinctive composition has led to the widely accepted view that MORB originate from a generally compositionally homogeneous and well-mixed upper mantle [*Allègre et al.*, 1983; *Hofmann*, 2003; *Sims and Hart*, 2006]. Unlike MORB, ocean island basalts (OIB) occur as tholeiitic and alkalic basalts that are variably enriched in highly incompatible elements. They are more isotopically heterogeneous and more radiogenic, e.g., higher in Sr and Pb, but lower in Nd isotopic ratios, than MORB and, thus, must be coming from a heterogeneous and less depleted mantle source [*Hofmann*, 2003; *White*, 2010, and references therein].

The most popular hypothesis for the origin of OIB is the hotspot or plume hypothesis, which originated from the concept that intraplate volcanoes are formed by magmas erupted through oceanic plates moving over stationary heat sources [*Wilson*, 1963]. *Morgan* [1972] further postulated the whole mantle is convecting, producing a global array of mantle plumes that originate from the core-mantle boundary. In this model, mantle plumes represent upwelling limbs of mantle

convection that funnel magmas at hotspots.

Radiogenic isotopic ratios (e.g., $^{87}Sr/^{86}Sr$, $^{143}Nd/^{144}Nd$, $^{206}Pb/^{204}Pb$) of oceanic basalts provide invaluable information on the composition of the Earth's mantle. Their heterogeneity represents the presence of compositionally distinct mantle regions that individually experience long time-integrated fractionation of the radioactive parentradiogenic daughter element pairs [e.g. Rb-Sr, Sm-Nd, U-Pb; *Gast et al.*, 1964; *Kay et al.*, 1970; *Weis et al.*, 2011]. *Zindler and Hart* [1986] proposed that ranges of isotopic compositions of oceanic basalts, especially of OIB, could be viewed as mixtures among several end-member components that reside in these distinct mantle regions and represent extremes of the observed isotopic values. Moreover, signals from ancient oceanic crust, sediment and even continental crust, identified through detailed investigations, motivated geochemists to link such isotope heterogeneity to deep crustal recycling [e.g. *Hofmann and White*, 1982; *Hofmann*, 1997, 2003]. Accordingly, the extreme ranges of Sr-Nd-Pb isotopic values of OIB represent distinct end-member mantle components. These include high '$\mu$' ($\mu = ^{238}U/^{204}Pb$; "HIMU"), or HIMU plus enriched mantle 1 (EM1) and 2 (EM2) end-members and may represent recycled oceanic crust and sediment [*Zindler and Hart*, 1986]. The Sr-Nd-Pb isotopic variations of these proposed end-members and proposed geochemically depleted mantle source of MORB (DMM) create a mantle tetrahedron in three-dimensional space [*Hart et al.*, 1992]. Inside the tetrahedron lies a common or focus zone (FOZO) where all components appear to converge [*Hart et al.*, 1992]. The end-member components apparently retain their isotopic distinction by lack of homogenization or equilibration with ambient mantle. Thus, the plume hypothesis originally posited the existence of an enriched and compositionally heterogeneous lower mantle that is separated from the upper, homogeneous mantle source of MORB although later results show that this is an

oversimplification [*Hofmann*, 2003; *White*, 2010].

Noble gases provide another excellent source of information on mantle geochemistry because of their inert nature and trace amounts in Earth. Among the noble gases, He analyses of MORB and OIB are the most abundant and early reports of high-$^3He/^4He$ ratios ($> 8\pm 1$ $R_A$, the nominal MORB value; $R_A$ value relative to air $^3He/^4He = 1.39 \times 10^{-6}$) in Hawaiian lavas had been used to bolster the deep mantle origin of OIB [*Craig and Lupton*, 1981; *Kurz et al.*, 1982; *Farley et al.*, 1992]. This is based on the idea that portions of the lower mantle have not yet undergone mixing or degassing and/or possibly still have near-primordial composition [*Craig and Lupton*, 1981].

Investigations of the relationship between He with Sr-Nd-Pb isotopes show that there is a general co-variance of these parameters in OIB [*Zindler and Hart*, 1986; *Farley et al.*, 1992; *Hilton et al.*, 1997]. To explain this relationship, the plume model evolved to include a common deep mantle component with high-$^3He/^4He$ characteristics, first termed the 'primitive helium mantle' (PHEM) with high-$^3He/^4He$ and near-primitive Sr-Nd-Pb isotopic compositions [*Farley et al.*, 1992]). Later workers positioned the high-$^3He/^4He$ source in the aforementioned FOZO or component 'C' and showed that it does not have a primitive composition [*Hart et al.*, 1992; *Hanan and Graham*, 1996; *Hilton et al.*, 1997; *Stracke et al.*, 2005]. Thus, high-$^3He/^4He$ OIB offer unique insights into the magma source and evolution of ocean island volcanism.

Many South Pacific OIB exhibit ranges of compositions that can be described simply as products of binary mixing between two mantle sources. For example, *Hoernle et al.* [2000] examined lavas from the Galápagos Islands formed during the last ∼14 m.y. and concluded that their asymmetrical surface horseshoe pattern of enriched and depleted chemical zonation reflects spatial heterogeneity within

their lower mantle plume source. Geochemical trends of the 3000-km long Easter and Salas y Gomez island chain are also consistent with two-component mixing between a MORB-like source and more enriched plume source [*Cheng et al.*, 1999].

The east-west trending Juan Fernandez volcanic chain in the southeast Pacific (Fig. 1.1) is no exception to this concept. It is one of the early foci of He studies [*Farley et al.*, 1993; *Farley*, 1991]. Lavas from these islands have $^{3}He/^{4}He$ values between 7.8 and 18.0 $R_A$, positioning Juan Fernandez among notable island chains with high-$^{3}He/^{4}He$ ratios. Similar to Hawaii and Iceland, an early popular explanation is that Juan Fernandez volcanoes were formed by the surface expression of a stationary mantle plume. In this particular case, the eastward moving Nazca plate travels over the Juan Fernandez plume, creating new volcanoes in the west and cutting off supply to older ones in the east [*Baker et al.*, 1987; *Farley*, 1991; *Farley et al.*, 1993]. Significantly, *Farley et al.* [1993] noted a chemical transition, mainly indicated by $^{3}He/^{4}He$ratios, from an enriched plume source in shield lavas (e.g. Loihi with respect to Hawaiian plumes, see *Kurz et al.*, 1983), to a depleted MORB-like source (i.e., DMM) in post-shield lavas.

Results of early investigations, however, also showed fairly homogeneous Sr-Nd(-Pb) (Pb isotopic analyses were very limited) isotopic ratios of Juan Fernandez lavas despite a diversity of $^{3}He/^{4}He$ ratios [*Gerlach et al.*, 1986; *Farley*, 1991; *Farley et al.*, 1993]. In other words, Juan Fernandez lavas show very limited to no co-variation between He and Sr-Nd(-Pb) isotope ratios that is commonly observed in several other high-$^{3}He/^{4}He$ OIB, with the highest values roughly converging toward the aforementioned PHEM, FOZO or C mantle component [e.g. *Farley et al.*, 1993; *Hanan and Graham*, 1996; *Hilton et al.*, 1999; *Castillo et al.*, 2007]. Thus, although the bimodal distribution of $^{3}He/^{4}He$ ratios tends to support the case for binary mixing, previous studies on Juan Fernandez could not effectively

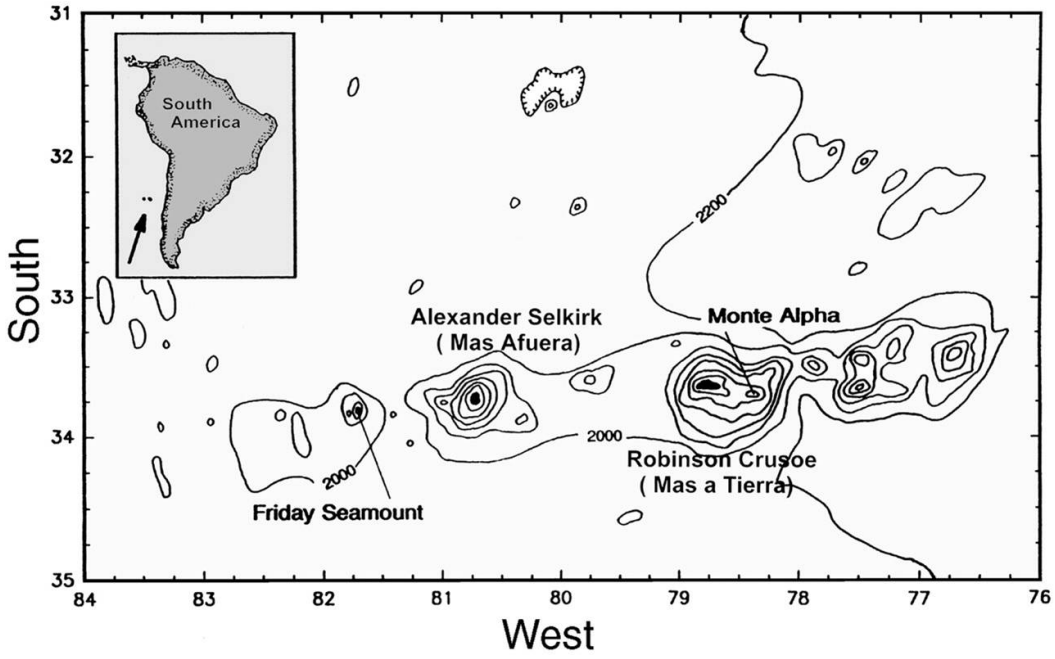


**Figure 1.1**: Bathymetric map of Juan Fernandez Islands from *Farley et al.* [1993].

define other geochemical arrays that are consistent with mixing between an enriched plume source and DMM, especially in view of such nearly homogeneous Sr-Nd(-Pb) ratios. Moreover, (*Natland*, 2003; see also, *Eiler et al.*, 1997) argued that the high-$^3$He/$^4$He lavas in Juan Fernandez result from the incorporation in crystallizing olivine of high-$^3$He gas pervading magma conduits and storage reservoirs. This notion is consistent with the counter-proposal that OIB geochemical composition, including high-$^3$He/$^4$He ratios, is not definitive of distinct mantle reservoirs and there is no direct connection between the deep mantle and surface lavas [*Foulger*, 2011, and references therein)].

Thus, the occurrence of both enriched and MORB-like $^3$He/$^4$He in Juan Fernandez is useful to our understanding of the origin of high-$^3$He/$^4$He OIB because its lava suites contain unexpectedly ambiguous pieces of information that may support arguments for either a high-$^3$He mantle plume signal, or non-systematic

isotopes with no correlations between He and other lithophile tracers. For the latter, *Natland* [2003] suggested that the high-$^3$He olivines are actually xenocrysts and the bulk rock composition of Juan Fernandez does not represent lower mantle source lithologies. So far, Sr-Nd(-Pb) isotopic composition of Juan Fernandez lavas does not distinguish clearly between the two possibilities of a real plume signal, or 'decoupling' of He from lithophile tracers.

The main objective of this study is to further document the geochemical characteristics of Juan Fernandez lavas. The main analytical emphasis is on complementary trace element and Pb isotopic compositions of the same lavas previously analyzed by *Farley et al.* [1993]. With the new analyses, the volcanic evolution, petrogenesis and mantle source of Juan Fernandez Islands are presented through coupled Sr-Nd-Pb isotopes plus major-trace element geochemistry and using concepts and ideas on mantle composition and dynamics that are more recent than those used by *Farley et al.* [1993] on mantle composition and dynamics [e.g. *Eiler et al.*, 1997; *Stracke et al.*, 2005; *Jackson et al.*, 2007, 2008; *Hofmann*, 2003; *White*, 2010; *Peters and Day*, 2014; *Castillo*, 2015]. The new results will greatly complement those of future detailed studies, such as studies on volatiles including $CO_2$ and other noble gases in Juan Fernandez lavas, to fully resolve the uncertainty regarding the high-$^3$He/$^4$He signature of Juan Fernandez lavas.

## 1.1 Geologic Background

The Juan Fernandez volcanic chain is an east-west trending group of islands and seamounts located at latitude 34°S in the southeast Pacific, some 660 km west of the Chilean coast (Fig. 1.1). The chain of islands and seamounts spans ∼800 km on the Nazca Plate that has an early Oligocene crustal age [*Baker et al.*,

1987; *Corvalan*, 1981]. It is comprised of two main islands, a small island and a few seamounts [*Baker et al.*, 1987]. The two main islands, about 180 km apart, are named Robinson (R.) Crusoe (formerly Mas a Tierra, closer to the land) and Alexander (A.) Selkirk (Mas Afuera, away from the land). In addition to the islands, two submarine volcanoes lie west of A. Selkirk, but little is known about their geology, and their discoveries were recent. Friday Seamount was discovered and first documented by *Farley* [1991], and Domingo Seamount, which lies further westward of Friday, was discovered and described by *Devey et al.* [2000].

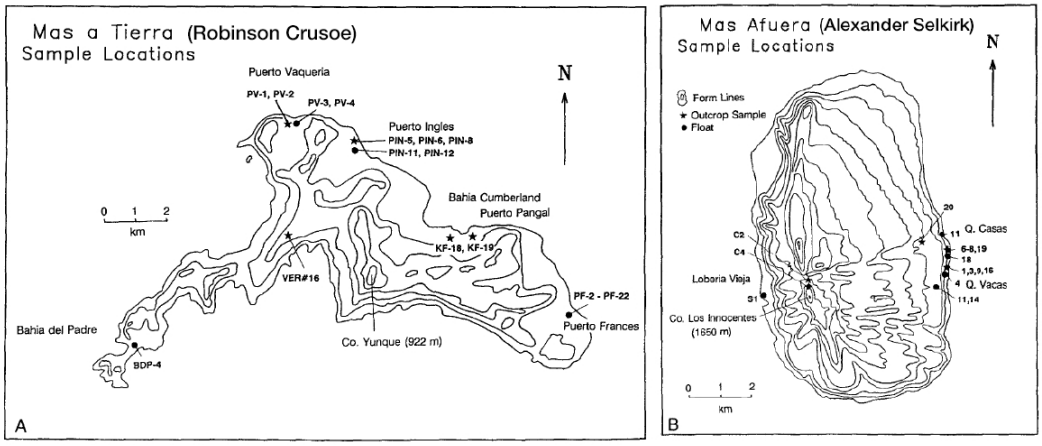


**Figure 1.2**: **A.** Modified map of Mas a Tierra/R. Crusoe from *Farley et al.* [1993] showing sample locations. **B.** Sample location map of Mas Afuera/A. Selkirk. Locations from which samples were collected are indicated by stars for outcrop samples and circles from boulders, talus, and cobbles. Prominent geographic features are labeled.

The stratigraphy of the islands is poorly known and, thus, volcano age is assumed to be the oldest radiometric date on each island [*Gripp and Gordon*, 2002]. Radiometric (K-Ar) ages range from 4.0-3.1 Ma for R. Crusoe. The oldest lavas from R. Crusoe are from Cumberland Bay, where a stratigraphically low sample was dated at 4.0 $\pm$ 0.2 Ma [*Baker et al.*, 1987]. Ages range from 2.5-0.85 Ma for A. Selkirk [*Booker et al.*, 1967; *Baker et al.*, 1987; *Farley et al.*, 1993]. Presumed oldest samples from R. Crusoe were identified by *Baker et al.* [1987] as from three

volcanic centers near Cumberland Bay: nearby Puerto Ingles (Central), and along the northern limb of the island Puerto Vaqueria (Peripheral), and Puerto Frances (Peripheral). Overall, radiometric dating has produced results consistent with age-progressive volcanism toward the east.

Dredged samples of fresh basalt suggest the two seamounts, Friday and Domingo are younger than A. Selkirk [*Farley et al.*, 1993]. Though neither seamount has radiometrically-determined ages , *Devey et al.* [2000] noted that the larger Friday seamount appears morphologically evolved with evidence of volcanic activity over a broad area and is likely to be older than Domingo. Furthermore, Domingo lies westward of Friday and has less sediment cover [*Devey et al.*, 2000]. Thus, the nature of samples and observational data for the seamounts are also consistent with the proposed eastward age-progression of volcanism in the Juan Fernandez volcanic chain [*Farley et al.*, 1993; *Devey et al.*, 2000]. *Baker et al.* [1987] initially classified eight groups of Juan Fernandez lavas based on geographic distribution of the different rock units, which were then combined with geochemical criteria to generalize two broad groups in R. Crusoe - central and peripheral. The R. Crusoe central and all A. Selkirk lavas consist of picritic basalts, aphyric alkalic basalts and quartz tholeiites. The R. Crusoe peripheral group includes olivine tholeiites, alkali basalts and basanites.

In this study, the classification scheme of *Farley et al.* [1993] is adopted to avoid confusion. Based on CIPW normative mineralogy, Juan Fernandez lavas consist of olivine tholeiites, alkali basalts and basanites. Furthermore, island samples belonging to distinct volcanic lineages can be identified using Ba/Zr as a discriminant, producing groups I, II, and III [*Farley et al.*, 1993]. Groups I and II consist of basalts and basanites, respectively, from R. Crusoe. Group III consists of A. Selkirk basalts, which are lithologically and chemically similar to group I

[see also *Baker et al.*, 1987]. Though not included in this study, *Farley et al.* [1993] also devised group IV, represented by one Friday seamount alkali basalt, which is chemically similar to alkali basalts, found on both islands. *Devey et al.* [2000] later reported that Friday is composed of basalts and basaltic trachyandesites whereas the Domingo rock suite consists of basanites.

## 1.2 Samples

In this study, a suite of samples from the two islands, R. Crusoe and A. Selkirk were analyzed. They were collected from the two main islands during Leg 1 of Scripps Institution of Oceanography (SIO)'s HYDROS expedition in November 1988. R. Crusoe samples are cobbles found in a valley or dike outcrop (Fig. 1.2A). Samples from A. Selkirk were mostly sampled from the large sea cliffs, a talus slope and beach (Fig. 1.2B). For all samples used in this study, previously determined major  select trace element compositions, petrographic and field descriptions and all He plus almost all Sr-Nd isotopic data are available in the literature [*Farley*, 1991; *Farley et al.*, 1993].

*Farley et al.* [1993] claimed that the samples are representative of the petrologic diversity of the exposed lavas in the islands, as they were collected from beaches, cliffs and dike outcrops. However, the samples were limited to basaltic lavas as the fieldwork may have been biased to find samples with abundant and fresh olivine phenocrysts for noble gas analysis. As a result, the sample suite may have been skewed towards picritic compositions. It is also noteworthy that the samples were collected in 1988, before the names of the islands were officially changed. Thus, samples collected from Mas Afuera (A. Selkirk) and Mas a Tierra (R. Crusoe) were prefixed with initials MF and MT, respectively. In this study, the

original sample names are adopted, again to avoid confusion.

The sample suite consists of group I basalts and group II basanites from R. Crusoe, and Group III basalts from A. Selkirk. It does not include central group lavas of the estimated oldest volcanic center of R. Crusoe, Bahia Cumberland [*Baker et al.*, 1987]. As noted earlier, however, our sample suite includes the three other volcanic centers along the northern limb of R. Crusoe. Specifically, group I includes two olivine tholeiites of the central group from Puerto Ingles and seven olivine tholeiites and alkali basalts from Puerto Vaqueria and Puerto Frances, all belonging to the peripheral group of *Baker et al.* [1987]. Group II includes four basanites, one from Puerto Vaqueria and three from Puerto Frances, from the peripheral group of *Baker et al.* [1987].

Groups I and III basalts represent the shield building stages in the respective islands. A total of 45 samples from all four groups were analyzed for $^{3}He/^{4}He$ values by *Farley* [1991]. Of the original 45 samples, 17 whole rock mafic samples (nine from R. Crusoe and eight from A. Selkirk) were selected for this study. They nearly represent the range of $^{3}He/^{4}He$ (7.8-17.2 $R_A$; the sample with the highest $^{3}He/^{4}He$=18 $R_A$, from an R. Crusoe olivine tholeiite is not included in this study. Although the samples that *Farley et al.* [1993] analyzed were primarily for He isotopes, these were also analyzed by XRF methods for major and several trace elements and by mass spectrometry for Sr-Nd isotopes. Some of these lavas were also analyzed for $\delta$ $^{18}O$ isotopes on olivine by *Eiler et al.* [1997].

It is important to note that although *Farley* [1991] proposed that group II basanites are post-erosional, these samples are beach cobbles. In contrast, *Baker et al.* [1987] observed that basanites occur as minor intrusives cutting into underlying shield-building group I lavas in R. Crusoe. Moreover, *Gerlach et al.* [1986] reported that basanites occur mostly as parasitic cones along the southwest

peninsula and represent the most recent activity on R. Crusoe. Thus, groups I and II lavas most likely represent the shield and post-shield stages of volcanism, respectively, in R. Crusoe and are the rough equivalent of the central and peripheral lava groups of *Baker et al.* [1987].

Group I olivine tholeiites are typically vesicular, containing 5-10% olivine phenocrysts that range in size from 0.5-1cm [*Farley et al.*, 1993]. Group I alkali basalts contain 10% olivine phenocrysts up to 1 cm in size. Group II basanites are also porphyritic and contain olivine and some clinopyroxene phenocrysts. Group III olivine tholeiites and one alkali basalt have porphyritic to saccharoidal texture and contain 5-30% olivine phenocrysts. Olivine phenocrysts range in size from 0.5-1 cm, except for those in a glassy flow, which are generally smaller (ca. 0.1 cm).

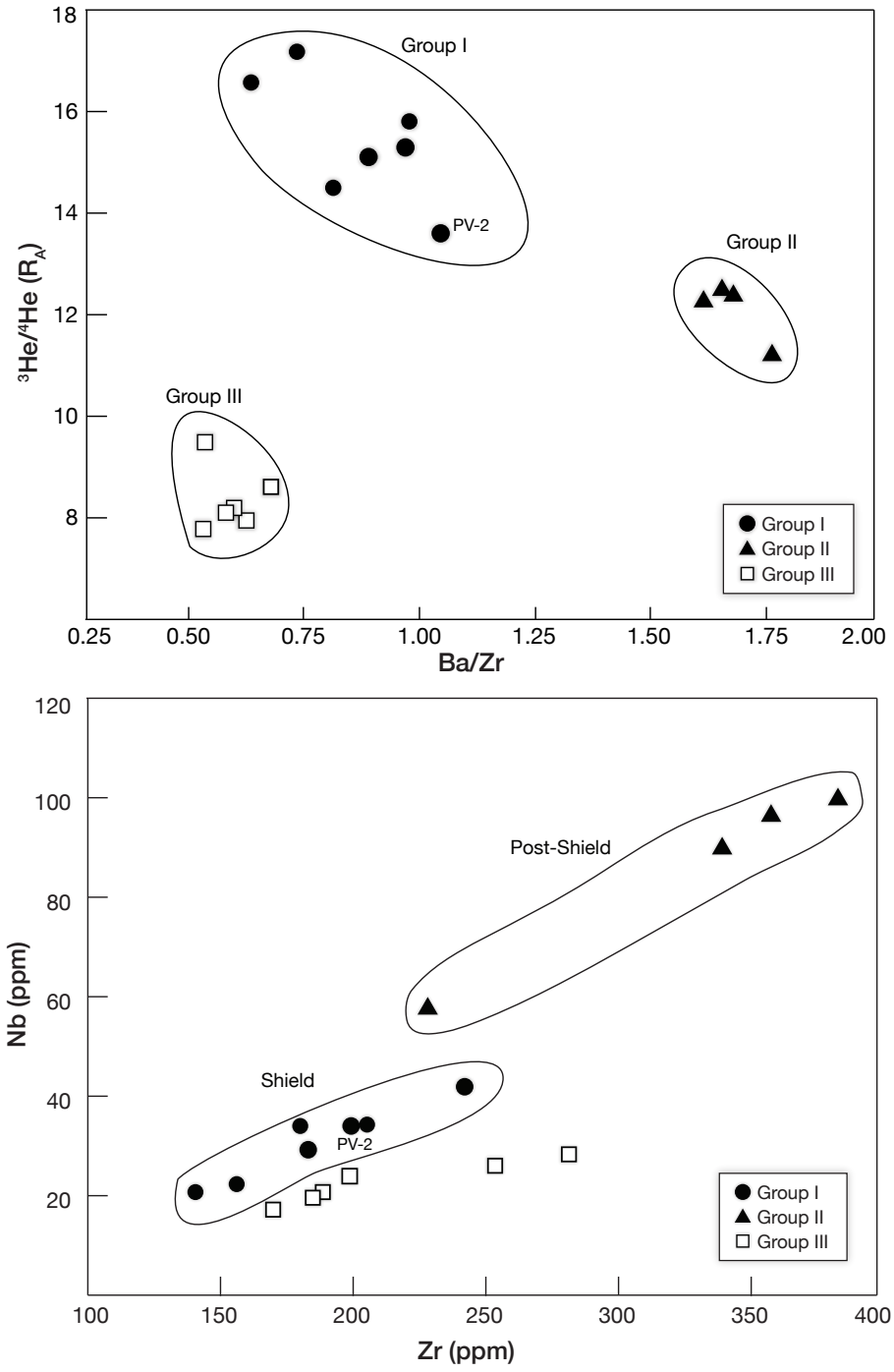


**Figure 1.3**: **A.** $^3He/^4He$ ($R_A$) versus Ba/Zr discrimination plot for mafic lavas suite from Juan Fernandez Islands, adapted from *Farley et al.* [1993], showing three rock groups I, II and III. **B.** Nb (ppm) versus Zr (ppm) diagram. PV-2 is a group II basanitoid.

# 2 Methods and Results

## 2.1 Analytical Methods

Seventeen whole rock mafic lavas were analyzed for abundances of trace elements Rb, Sr, Y, Ba, Pb, Th, rare earth elements (REE), and high field-strength elements (HFSE) Nb, Ta, Zr, Hf, for their Pb isotopic composition. The Sr and Nd isotopes were also analyzed for one sample (PF-21) to replicate findings by *Farley* [1991], and for three samples (PF-3, MF-16, MF-6) that were missing in the *Farley et al.* [1993] original subset. All radiogenic isotope analyses were performed on whole-rock samples. Finally, Nd isotopes of olivine separates from five samples (MF-3, PF-21, PF-5, PF-10, PIN-8) spanning the range of $^{3}He/^{4}He$ ratios from 7.8-18.0 $R_A$ were also analyzed.

Prior to analysis, samples were examined to identify fresh portions. The rock portions were then crushed to cm size fragments, ultrasonically cleaned in a $\sim$5% $HNO_3$ solution and dried in an oven at $\sim$110°C. Once dried, the fragments were powdered in an alumina ceramic shatterbox. Trace elements were determined by inductively-coupled plasma mass spectrometry (ICP-MS) using a ThermoQuest Element 2 instrument. Strontium, Nd and Pb isotopes were analyzed through thermal ionization mass spectrometry (TIMS) using a Micromass VG 54 Instrument. The sample digestion procedure used for the ICP-MS and TIMS analyses is similar

to that described in *Janney and Castillo* [1996]. About 20 mg of sample powder was dissolved in a clean teflon beaker using a doubly-distilled HF:$HNO_3$ (2:1) mixture, dried over a hotplate, and evaporated twice in concentrated HNO3. For the trace element analysis, the dissolved sample was diluted ∼4000X with a 1% $HNO_3$ solution containing 1 ppb $^{115}$In as an internal standard to correct for signal run intensity variation and instrumental drift.

For Pb, Sr and Nd isotope analysis, each sample was dissolved as above and then re-dissolved in 4.5 N HCl, dried, then dissolved again in 2.5 N HBr, dried, and finally passed through a cation column in a HBr medium to collect Pb. The left-over sample solution from the Pb column was dried and loaded onto a primary cation column in a HCl medium to collect Sr and REE. Finally, the REE cut was passed through an ion exchange column in an alpha HIBA (alpha-hydroxyisobutyric) acid medium to collect Nd.

Olivine separates analyzed for Nd isotopes were hand picked under a binocular microscope from aliquots of the cm-sized fragments of whole rock samples prepared by *Farley* [1991]. Approximately 70 mg of separates were then ultrasonically cleaned with a 1% $HNO_3$ solution and dried in an oven at ∼110°C prior to dissolution. The olivine separates were dissolved in the same way as the whole rock samples. The separates were not crushed prior to dissolution. Neodymium was collected from the sample solution as described above.

Additional details of the analyses plus analytical uncertainties are reported as footnotes accompanying appropriate tables.

**Table 2.1**: Trace Element abundance data for Juan Fernandez lavas

| **Sample** | **PV-2** | **PV-4** | **PF-3** | **PF-5** | **PF-10** | **PIN-12** | **PIN-8** | **PF-16** | **PV-1** |
|---|---|---|---|---|---|---|---|---|---|
| Group | I | I | I | I | I | I | I | II | II |
| Rock type[1] | BSD | O.T. | A.B. | A.B. | O.T. | O.T. | O.T. | BSN | BSN |
| Rb (ppm) | 8 | 15 | 7 | 21 | 16 | 6 | 2 | 38 | 58 |
| Ba | 208 | 169 | 164 | 236 | 177 | 100 | 104 | 403 | 616 |
| Nb | 34 | 34 | 29 | 42 | 34 | 22 | 21 | 58 | 100 |
| Sr | 584 | 388 | 412 | 540 | 425 | 317 | 319 | 661 | 932 |
| Zr | 198 | 205 | 183 | 242 | 180 | 156 | 141 | 228 | 383 |
| Y | 16 | 21 | 17 | 20 | 20 | 16 | 15 | 29 | 37 |
| La | 8.47 | 20.08 | 9.78 | 15.91 | 14.31 | 9.1 | 7.4 | 32.99 | 56.52 |
| Ce | 19.65 | 42.86 | 21.7 | 34.77 | 30.01 | 20.2 | 16.55 | 63.98 | 107.55 |
| Pr | 2.91 | 5.67 | 3.07 | 4.57 | 4.21 | 2.75 | 2.42 | 8.15 | 13.56 |
| Nd | 13.08 | 23.01 | 12.86 | 18.79 | 17.83 | 11.25 | 10.78 | 31.15 | 48.96 |
| Sm | 3.6 | 5.47 | 3.5 | 4.59 | 4.48 | 2.93 | 3.06 | 6.87 | 9.8 |
| Eu | 1.79 | 1.92 | 1.59 | 1.91 | 1.81 | 1.19 | 1.29 | 2.5 | 3.43 |
| Tb | 0.52 | 0.74 | 0.52 | 0.64 | 0.69 | 0.45 | 0.47 | 0.94 | 1.3 |
| Dy | 4.91 | 3.68 | 3.2 | 3.68 | 4.11 | 2.85 | 3.2 | 4.36 | 5.57 |
| Ho | 0.6 | 0.8 | 0.62 | 0.68 | 0.75 | 0.55 | 0.56 | 1.01 | 1.3 |
| Er | 1.61 | 2.1 | 1.68 | 1.79 | 2.01 | 1.48 | 1.52 | 2.78 | 3.65 |
| Yb | 1.24 | 1.57 | 1.32 | 1.3 | 1.58 | 1.09 | 1.15 | 2.08 | 2.9 |
| Lu | 0.18 | 0.22 | 0.19 | 0.19 | 0.22 | 0.16 | 0.16 | 0.31 | 0.42 |
| Hf | 4.4 | 4.48 | 4.12 | 5.16 | 4.11 | 3.52 | 3.31 | 4.79 | 7.56 |
| Ta | 2.11 | 2.07 | 1.81 | 2.41 | 2.06 | 1.39 | 1.33 | 3.29 | 5.64 |
| Pb | 1.13 | 1.66 | 1.25 | 1.82 | 1.65 | 0.8 | 0.75 | 2.68 | 4.55 |
| Th | 1.9 | 2.46 | 2.19 | 2.45 | 1.93 | 1.4 | 1.25 | 4.75 | 8.1 |
| U | 0.59 | 0.78 | 0.33 | 0.93 | 0.43 | 0.27 | 0.17 | 1.09 | 1.89 |
| Ba/Zr | 1.05 | 0.82 | 0.9 | 0.98 | 0.98 | 0.64 | 0.74 | 1.76 | 1.61 |
| Nb/Zr | 0.17 | 0.17 | 0.16 | 0.17 | 0.19 | 0.14 | 0.15 | 0.25 | 0.26 |
| La/Yb | 6.85 | 12.78 | 7.39 | 12.22 | 9.04 | 8.36 | 6.46 | 15.86 | 19.5 |

**Table 2.1:** Trace Element abundance data for Juan Fernandez lavas, Continued

| **Sample** | **PF-21** | **PF-17** | **MF-C4** | **MF-3** | **MF-16** | **MF-6** | **MF-S1** | **MF-C2** |
|---|---|---|---|---|---|---|---|---|
| Group | II | II | III | III | III | III | III | III |
| Rock type[1] | BSN | BSN | O.T. | O.T. | O.T. | O.T. | A.B. | O.T. |
| Rb (ppm) | 55 | 44 | 20 | 12 | 13 | 13 | 13 | 9 |
| Ba | 599 | 559 | 150 | 106 | 111 | 110 | 137 | 136 |
| Nb | 97 | 90 | 28 | 17 | 21 | 20 | 24 | 26 |
| Sr | 862 | 825 | 381 | 320 | 391 | 393 | 382 | 360 |
| Zr | 357 | 339 | 281 | 170 | 189 | 184 | 199 | 253 |
| Y | 32 | 30 | 29 | 20 | 18 | 21 | 19 | 16 |
| La | 50.64 | 44.09 | 17.87 | 12.17 | 8.54 | 10.49 | 11.94 | 6.93 |
| Ce | 97.44 | 85.42 | 35.38 | 26.56 | 18.72 | 23.23 | 25.53 | 15.47 |
| Pr | 11.78 | 11.2 | 5 | 3.97 | 2.78 | 3.47 | 3.83 | 2.24 |
| Nd | 41.73 | 41.39 | 20.82 | 17.12 | 12.15 | 15.26 | 16.01 | 9.97 |
| Sm | 8.5 | 8.59 | 5.48 | 4.56 | 3.45 | 4.26 | 4.16 | 3 |
| Eu | 2.96 | 3 | 2.4 | 1.61 | 1.49 | 1.71 | 1.65 | 1.94 |
| Tb | 1.12 | 1.13 | 0.82 | 0.69 | 0.54 | 0.65 | 0.59 | 0.49 |
| Dy | 5.64 | 6.78 | 5.18 | 4.34 | 3.39 | 4.32 | 3.52 | 3.73 |
| Ho | 1.07 | 1.08 | 0.99 | 0.78 | 0.68 | 0.79 | 0.67 | 0.63 |
| Er | 2.81 | 2.81 | 2.57 | 2.08 | 1.9 | 2.12 | 1.71 | 1.79 |
| Yb | 2.09 | 2.1 | 1.92 | 1.53 | 1.45 | 1.6 | 1.32 | 1.46 |
| Lu | 0.3 | 0.29 | 0.28 | 0.22 | 0.22 | 0.23 | 0.19 | 0.21 |
| Hf | 6.93 | 6.66 | 6.08 | 3.87 | 4.33 | 4.17 | 4.42 | 5.66 |
| Ta | 5.27 | 4.98 | 1.71 | 1.08 | 1.28 | 1.25 | 1.48 | 1.63 |
| Pb | 3.85 | 4.27 | 1.46 | 0.9 | 2.76 | 0.98 | 1.1 | 1.09 |
| Th | 7.77 | 6.61 | 2.6 | 1.5 | 1.34 | 1.29 | 1.61 | 2.12 |
| U | 1.65 | 1.41 | 0.66 | 0.39 | 0.38 | 0.35 | 0.41 | 0.45 |
| Ba/Zr | 1.68 | 1.65 | 0.53 | 0.63 | 0.59 | 0.6 | 0.69 | 0.54 |
| Nb/Zr | 0.27 | 0.27 | 0.1 | 0.1 | 0.11 | 0.11 | 0.12 | 0.1 |
| La/Yb | 24.27 | 21.01 | 9.29 | 7.95 | 5.87 | 6.55 | 9.06 | 4.76 |

**Table 2.2**: Sr-Nd-Pb isotope data for Juan Fernandez lavas

| **Sample** | **PV-2** | **PV-4** | **PF-3** | **PF-5** | **PF-10** | **PIN-12** | **PIN-8** | **PF-16** | **PV-1** |
|---|---|---|---|---|---|---|---|---|---|
| Group | I | I | I | I | I | I | I | II | II |
| Rock type[1] | BSD | O.T. | A.B. | A.B. | O.T. | O.T. | O.T. | BSN | BSN |
| $^{87}Sr/^{86}Sr$(2) | *0.70364* | *0.70344* | 0.703698 ±12 | *0.70339* | *0.70362* | *0.70349* | *0.70363* | *0.70344* | 0.70343 ±12 |
| $^{143}Nd/^{144}Nd$(2) | *0.51284* | *0.51286* | 0.512835 ±5 | *0.51287* | *0.51286* | *0.51282* | *0.51284* | *0.51288* | 0.51287 ± 6 |
| $^{143}Nd/^{144}Nd$ (OLV) | | | | 0.512808 ±14 | 0.512827 ± 9 | | 0.512824 ±9 | | |
| $^{206}Pb/^{204}Pb$ | 19.194 | 19.258 | 19.292 | 19.166 | 19.224 | 19.189 | 19.179 | 19.216 | 19.163 |
| $^{207}Pb/^{204}Pb$ | 15.666 | 15.675 | 15.669 | 15.647 | 15.678 | 15.653 | 15.638 | 15.631 | 15.656 |
| $^{208}Pb/^{204}Pb$ | 39.161 | 39.276 | 39.291 | 39.099 | 39.31 | 39.184 | 39.138 | 39.237 | 39.315 |

(1) BSD = basanitoid; BSN = basanite; A.B. = alkali basalt
(2) Values in italic are from *Farley et al.* [1993].

**Table 2.2:** Sr-Nd-Pb isotope data for Juan Fernandez lavas, Continued

| **Sample** | **PF-21** | **PF-17** | **MF-C4** | **MF-3** | **MF-16** | **MF-6** | **MF-S1** | **MF-C2** |
|---|---|---|---|---|---|---|---|---|
| Group | II | II | III | III | III | III | III | III |
| Rock type[1] | BSN | BSN | O.T. | O.T. | O.T. | O.T. | A.B. | O.T. |
| $^{87}Sr/^{86}Sr$[2] | 0.70349 | *0.7034* | *0.70354* | *0.70354* | 0.703614 ±11 | 0.703601 ±12 | *0.70365* | *0.70355* |
| $^{143}Nd/^{144}Nd$[2] | 0.51288 | *0.51286* | *0.51287* | *0.51289* | 0.51288 ±5 | 0.512869 ±14 | *0.51287* | *0.51288* |
| $^{143}Nd/^{144}Nd$ (OLV) | 0.512837 ±9 | | | 0.512886 ±32 | | | | |
| $^{206}Pb/^{204}Pb$ | 19.182 | 19.184 | 19.177 | 18.939 | 19.228 | 19.170 | 19.081 | 19.158 |
| $^{207}Pb/^{204}Pb$ | 15.637 | 15.635 | 15.657 | 15.632 | 15.684 | 15.649 | 15.636 | 15.652 |
| $^{208}Pb/^{204}Pb$ | 39.271 | 39.262 | 39.197 | 38.893 | 39.138 | 39.078 | 39.068 | 39.188 |

Strontium, Nd and Pb isotope ratios were analyzed using a 9-collector, Micromass Sector 54 thermal ionization mass spectrometer (TIMS). Total procedural blanks are 35 pg for Sr, 10 pg for Nd and 60 pg for Pb. Strontium isotopic ratios were fractionation-corrected to $^{86}Sr/^{88}Sr = 0.1194$ and are reported relative to $^{87}Sr/^{86}Sr$=0.710254 ± 0.000018 (n=22) for NBS 987 during the period of analysis. Neodymium isotopic ratios were measured in oxide form, fractionation corrected to $^{146}NdO/^{144}NdO = 0.72225$ ($^{146}NdO/^{144}NdO = 0.7219$) and reported relative to $^{143}Nd/^{144}Nd = 0.511856 \pm 0.000016$ (n = 19) for the La Jolla Nd Standard during the period of analysis. Lead isotopic ratios were analyzed using the double-spike method to correct for mass fractionation during analyses; separate measurements of spiked and unspiked samples were made on different aliquots from the same dissolution. The SBL-74 $^{207}Pb/^{204}Pb$ double-spike from the University of Southampton was used. During the analysis period, the method produced the following results for NBS981: $^{206}Pb/^{204}Pb = 16.930 \pm 0.002$, $^{207}Pb/^{204}Pb = 15.4896 \pm 0.0027$ and $^{208}Pb/^{204}Pb = 36.6999 \pm 0.0086$ (n = 11); in-run uncertainties are better than these true errors.

## 2.2 Results

### 2.2.1 Trace Elements

Table 2.1 lists the trace element composition of the samples analyzed. These consist of four olivine tholeiites (group I), 2 alkali basalts (group I) and five basanites (group II) from R. Crusoe and five olivine tholeiites and an alkali basalt (group III) from A. Selkirk. Based on their Ba/Zr ratios, the samples belong to three distinct volcanic lineages [*Farley*, 1991; *Farley et al.*, 1993]. Group I have the lowest Ba/Zr ratios (0.75), group II have the highest ratio (1.8) and group III have an intermediate ratio ($\sim$ 1.1). The range of our new Ba/Zr ratios (0.53-1.76) is slightly lower than that of Farley and co-workers (0.75-1.80), but consistently defines the same groupings (1.3. The only exception is sample PV-2, which was not previously analyzed for Ba/Zr, but classified by Farley and co-workers as group II based on normative mineralogy. That is, although *Farley et al.* [1993] claimed that lavas with less than 5% normative nepheline are classified as basalt they designated PV-2, with 4.95%, as a basanite. However, the new results show that its Ba/Zr (1.05) value as well as other geochemical characteristics plot closer to group I basalts and, thus, it is classified henceforth as group I basanitoid that represents a transition between basalt and basanite.

The HFS elements Nb, Ta and Zr also highlight the distinction among Juan Fernandez lavas. The overall range of Zr/Nb (4-10) is consistent with low ratios in OIB (<10). Niobium correlates with Ta and Zr (Fig. 1.3). Group II has the highest Nb and Zr contents (>58 and >228 ppm, respectively) whereas groups I and III have overlapping lower values (<42 ppm Nb, <253 ppm Zr). However, group I has lower Nb for given Zr values than group II. Calculated Nb/Nb$^*$ values (Jackson et al., 2008) range from 1.36-2.87, with A. Selkirk group III basalts having the

lowest value. Calculated Ta/Ta* values range from 1.48-3.09; group III again has the lowest Ta/Ta* value. Calculated Ti/Ti* values range from 0.74-2.07 and are highest in group III.

Juan Fernandez samples show light-REE enriched concentration patterns typical of OIB (Fig. 2.1). Most of the samples plot within the range of previous REE analyses of *Baker et al.* [1987] and similarly display distinctions between the two islands. More specifically, distinctions among three groups are consistent with the three lava groups proposed by *Farley et al.* [1993]. Most samples reveal a slight Eu anomaly, which occurs when the Eu normalized-concentration is either enriched (positive anomaly) or depleted (negative anomaly) relative to adjacent REE. The Eu anomaly becomes more positive with increasing REE concentration within group I, which was probably generated at a relatively shallower depth, allowing plagioclase crystallization [*Sobolev et al.*, 2000]. The more chondrite-like group III samples from A. Selkirk display larger positive Eu anomalies than those from R. Crusoe. Shield-building basalts from both islands have similar average light- to medium-REE slopes, with group I $(La/Sm)_N = 1.94$ and group III $(La/Sm)_N = 1.73$, and lower than post-shield group II basanites $(La/Sm)_N = 3.50$. Overall the gradient of the normalized REE concentration patterns differs between the two lava groups from R. Crusoe. Group I represents the least fractionated suite, with an average $(La/Yb)_N = 9.0$, and group II being more fractionated with $(La/Yb)_N = 20.2$.

The primitive mantle-normalized spidergram (Fig. 2.2) shows the entire lava suite exhibits sub-parallel patterns that are enriched in highly incompatible elements, similar to OIB and different from depleted MORB. Groups I and III have nearly identical concentration patterns, but group II is distinctively more enriched in highly incompatible elements (e.g., Ba, Th up to ~90X primitive mantle), which

is consistent with the findings of *Baker et al.* [1987] and *Farley* [1991].

### 2.2.2 Radiogenic Isotopes

The Sr, Nd and Pb isotopic compositions of Juan Fernandez lavas are also listed in Table 2.1 and shown graphically in Figures 2.3 and 2.4. In general, there is very limited variation in $^{87}Sr/^{86}Sr$ (0.70339-0.70390) and $^{143}Nd/^{144}Nd$ (0.51282-0.51289) values, similar to previous results [*Farley*, 1991; *Farley et al.*, 1993; *Gerlach et al.*, 1986]. In detail, group I spans the entire range of $^{87}Sr/^{86}Sr$ values and on average, group II has the lowest (<0.70349) whereas group III has intermediate (0.70354-0.703650) values (Fig. 2.3). Group I also has the largest range of $^{143}Nd/^{144}Nd$ ratios but has lower values on average (<0.51286). Group II has a moderate range of $^{143}Nd/^{144}Nd$ (0.52186-0.51288) whereas group III has the highest $^{143}Nd/^{144}Nd$ (up to 0.51289). Overall, group I is relatively the most isotopically heterogeneous Juan Fernandez lava group in terms of Sr and Nd isotopic composition, spanning the most and least radiogenic values, group II completely overlaps its most depleted end, and group III is relatively homogeneous and generally depleted.

Table 2.1 also lists the Nd isotopic compositions of five olivine separates from at least one of each lava group, and range from 7.8-17.2 $R_A$ in $^{3}He/^{4}He$ ratios. The $^{143}Nd/^{144}Nd$ values measured on three olivine separates (PIN-8, MF-3, PF-10) are similar within analytical uncertainty (±16) to respective whole rock values whereas the other two (PF-5, PF-21) are within twice the uncertainty.

Figure 2.4 shows that the $^{206}Pb/^{204}Pb$, $^{207}Pb/^{204}Pb$, and $^{208}Pb/^{204}Pb$values of Juan Fernandez. *Gerlach et al.* [1986] previously reported the Pb isotopic ratios for R. Crusoe rocks as $^{206}Pb/^{204}Pb$= 19.042-19.214, $^{207}Pb/^{204}Pb$= 15.595-15.627, and $^{208}Pb/^{204}Pb$= 38.058-39.099. The ranges of the new data are $^{206}Pb/^{204}Pb$=

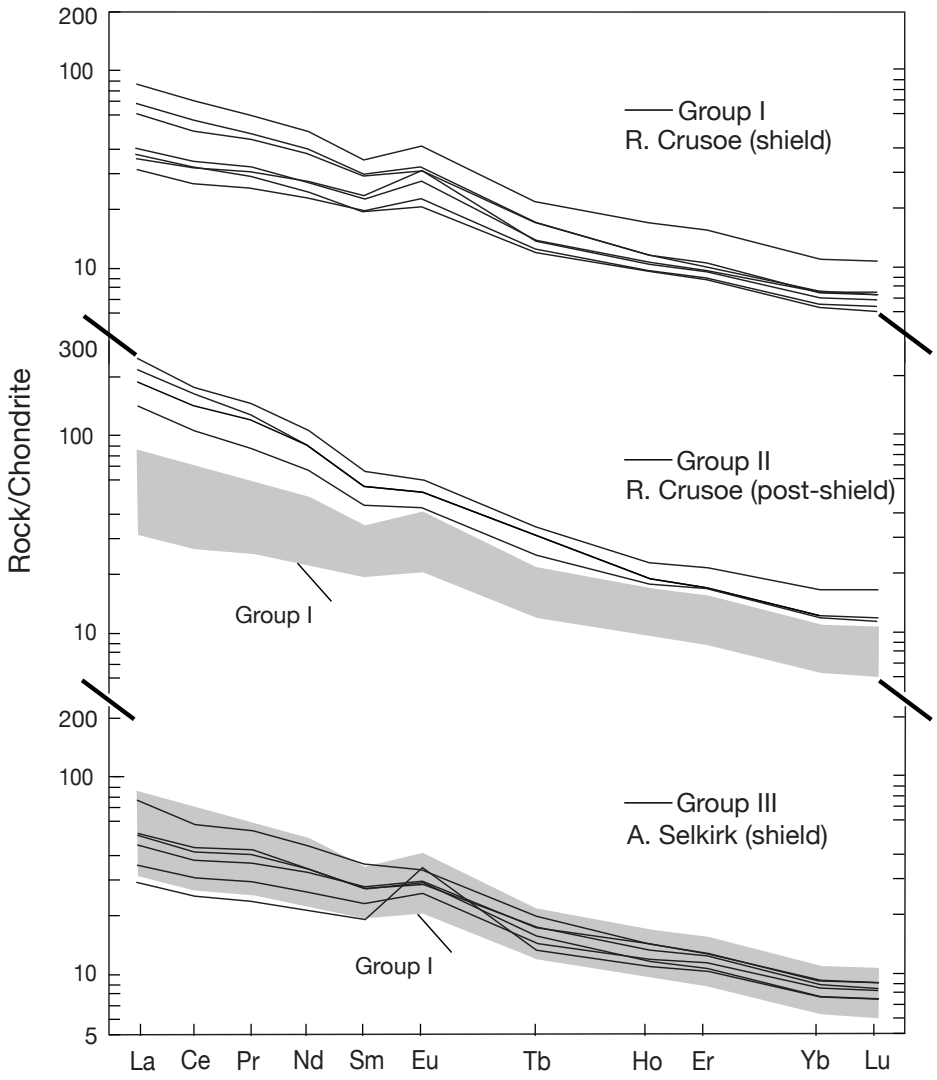


**Figure 2.1**: Chondrite-normalized REE concentration patterns of Juan Fernandez lavas. Shaded region is the range of values for group I. Chondrite normalizing values from *Sun and McDonough* [1989].

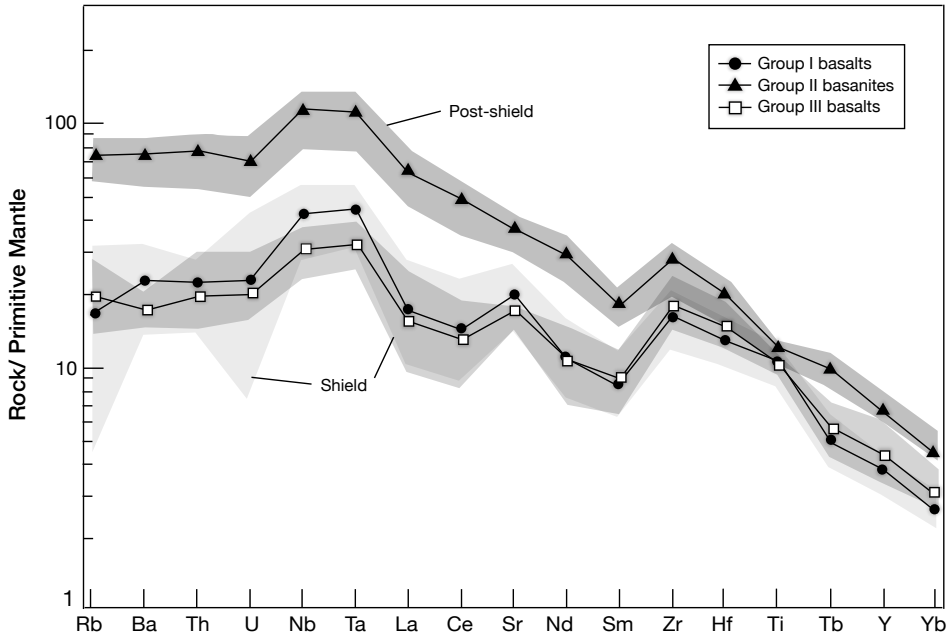


**Figure 2.2**: Primitive mantle-normalized incompatible trace element concentration patterns, shaded regions represent range of groups I-III Juan Fernandez lavas. Average concentrations are displayed with group-designated symbols. Data from *Farley et al.* [1993] are included. Normalizing values are from *Sun and McDonough* [1989].

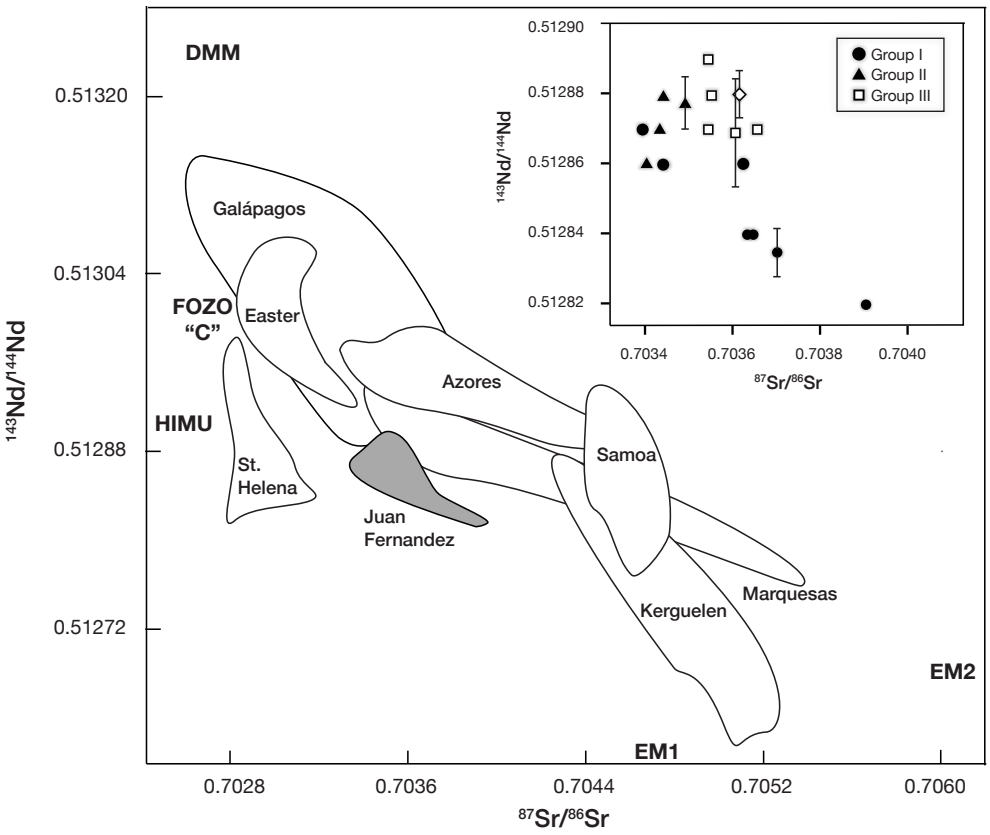


**Figure 2.3**: $^{143}Nd/^{144}Nd$ vs. $^{87}Sr/^{86}Sr$ diagram for Juan Fernandez lavas relative to some OIB. Inset shows the details of $^{143}Nd/^{144}Nd$ vs. $^{87}Sr/^{86}Sr$ ratios for Juan Fernandez Islands, including previous values from *Farley et al.* [1993]. See Table 2.1 for actual values. Samples (with $^{143}Nd/^{144}Nd$ uncertainty bars) PF-21, MF-16, MF-S1 and PF-3 were analyzed in this study.

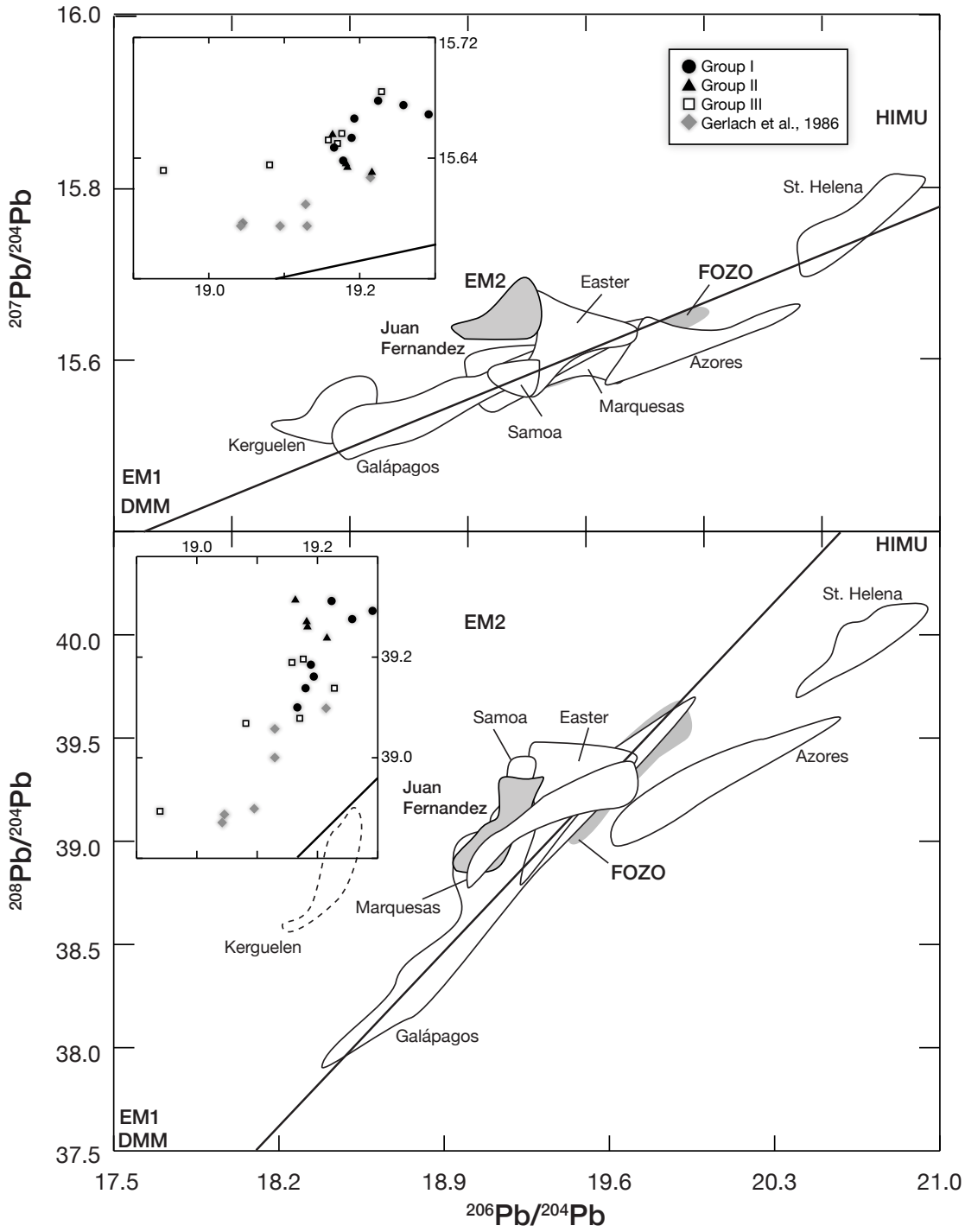


**Figure 2.4**: $^{206}Pb/^{204}Pb$-$^{207}Pb/^{204}Pb$and $^{206}Pb/^{204}Pb$-$^{208}Pb/^{204}Pb$ diagrams for Juan Fernandez lavas, from this study and *Gerlach et al.* [1986]. Fields for other OIB from the GEOROC database (http://georoc.mpchmainz.gwdg.de/georoc/) are shown for comparison. The locations of the four proposed mantle end-members DMM, HIMU, EM1, and EM2 are from *Zindler and Hart* [1986]; location of FOZO is from *Stracke et al.* [2005].

19.163-19.292, $^{207}Pb/^{204}Pb$= 15.631-15.678, and $^{208}Pb/^{204}Pb$= 39.099-39.315 for R. Crusoe lavas. Lead isotope ratios were also analyzed for A. Selkirk, which previously lacked any Pb isotopic analyses. $^{206}Pb/^{204}Pb$branges from 18.939-19.228, $^{207}Pb/^{204}Pb$= 15.632-15.684 and $^{208}Pb/^{204}Pb$= 38.893-39.197. As a whole, the Pb isotopic composition of Juan Fernandez is still relatively limited compared to neighboring San Ambrosio and San Felix islands [see also *Gerlach et al.*, 1986]. In detail, groups I and II completely overlap in $^{206}Pb/^{204}Pb$ and $^{208}Pb/^{204}Pb$ values, similar to their Sr and Nd isotopes, and are more radiogenic than group III. There is no apparent distinction among the groups in terms of $^{207}Pb/^{204}Pb$ ratios. Juan Fernandez Pb isotopic arrays lie parallel and above the northern hemisphere reference line (NHRL) and do not trend toward the depleted Pacific MORB mantle (DMM) source.

# 3 Discussion

Overall, the new trace element data confirm as well as strengthen the previously established chemical classification scheme for R. Crusoe and A. Selkirk lavas (Figs. 1.3, 2.1, 2.2) Combined Sr, Nd and Pb isotopic data are also consistent with the previously established limited isotopic variation of the lavas (Figs. 2.3 and 2.4). Such a limited range of Sr, Nd and Pb isotopic composition of Juan Fernandez lavas strongly suggests that the parental magmas for group I and III olivine tholeiites and alkalic basalts and group II basanites originated from a common mantle source with a slightly heterogeneous composition [*Farley et al.*, 1993]. Thus, to a first order the differences in the major and trace element compositions presented above can be ascribed to differences in the partial melting systematics of such a common mantle source.

The following sub-sections present interpretations regarding the origins of the major and trace element variation in Juan Fernandez lavas in light of their fairly limited Sr-Nd-Pb isotopic ratios. Based on these results, the mantle source of Juan Fernandez lavas is constrained and, finally, a geologic evolution of the Juan Fernandez volcanic chain that is consistent with the proposed plume hypothesis for the origin of the majority of OIB is proposed.

## 3.1 Major Element Variations

To a first order, the fairly coherent trends or liquid lines of descent in some of the MgO variation diagrams for Juan Fernandez lavas (Fig. 3.1) can be used to interpret that the compositional evolution of Juan Fernandez lavas. They show variation as a consequence of crystal-liquid fractionation processes, primarily partial melting and/or fractional crystallization. Specifically, the general linear trends between MgO and $SiO_2$, $TiO_2$, FeO* or CaO in primitive lavas (MgO $>\sim$4%) indicate a strong olivine fractionation control, either though accumulation or removal of olivine from a primitive magma composition. Moreover, the inflections of the trends in these diagrams with increasing differentiation (MgO $<\sim$4%) mark the onset of a new mineral (or set of minerals, e.g., clinopyroxene, plagioclase, titanomagnetite) that joins the fractional crystallization of olivine.

The larger variations of $Na_2O$, $K_2O$ or $P_2O_5$ with decreasing MgO, however, strongly indicate that partial melting also plays an important role in the generating the compositional evolution of Juan Fernandez lavas. That is, although individual lava groups display coherent trends that are consistent with fractional crystallization in each diagram, they also tend to form individual sub-trends that are most likely due to partial melting. These sub-trends are more evident in these diagrams involving Na, K and P because these are relatively more incompatible and, thus, their compositional evolutions are more sensitive to partial melting than the other major elements [e.g., *Shaw*, 1970].

*Klein and Langmuir* [1987] presented a widely adopted method to provide information on partial melting of the mantle from the major element composition of basaltic lavas. They used total FeO and $Na_2O$ (expressed as $Fe_8$ and $Na_8$, respectively, after normalizing to 8 wt % MgO in order to correct for the effects of 1 atm crystal fractionation) of MORB containing 5-8.5 wt % MgO to represent

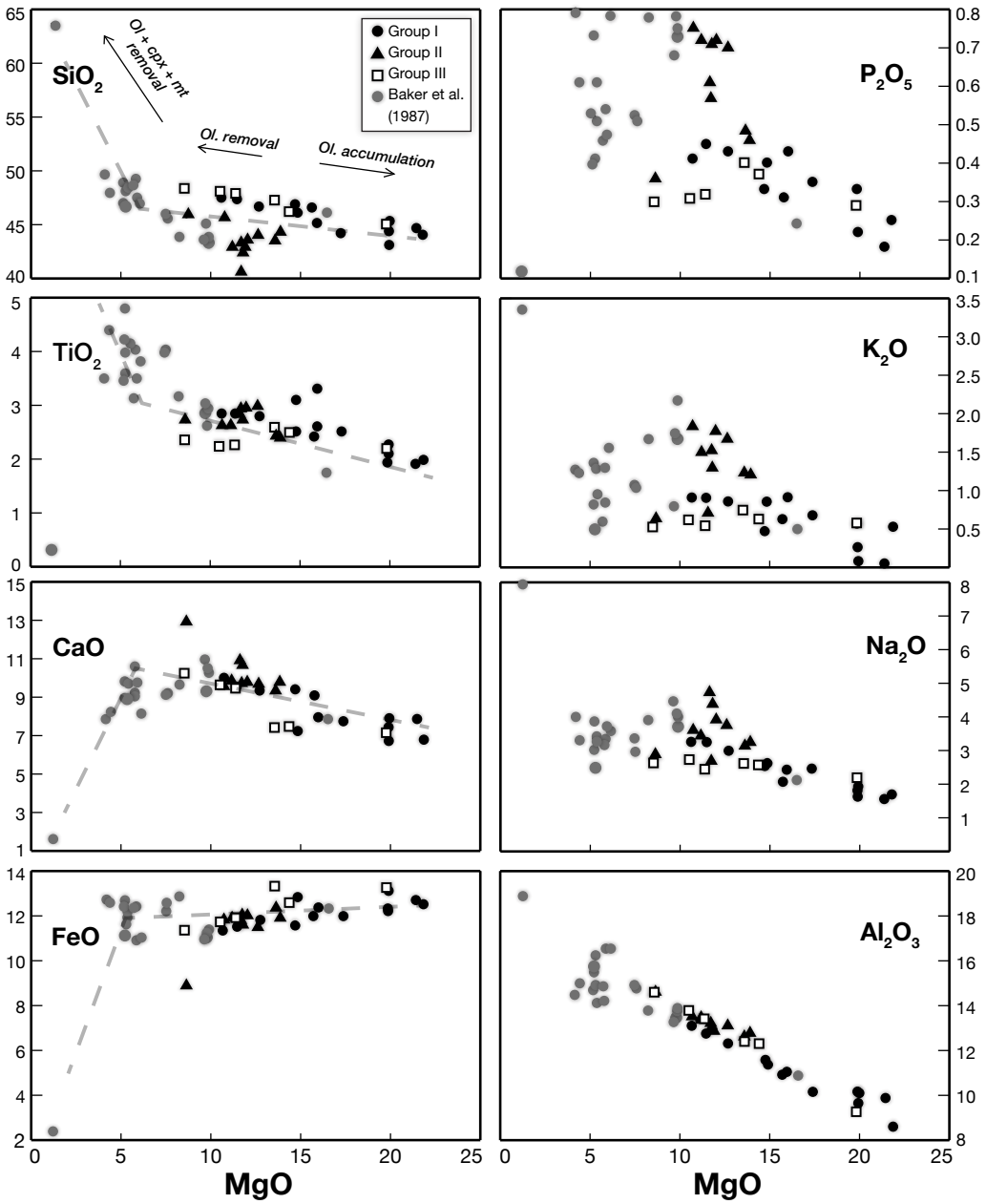


**Figure 3.1**: Variation of major oxides (wt %) as a function of MgO (wt. %) contents in Juan Fernandez lavas. Data include group I, II, and III lavas from *Farley et al.* [1993], and lavas from *Baker et al.* [1987]. See text for discussion..

differences in the degree and pressure of partial melting of their upper mantle source. The same concept is applied here in order to constrain the relative differences in the degree and pressure of partial melting of the common mantle source of Juan Fernandez lavas, but only qualitatively. This is because the sample suite is biased towards picritic compositions (9 - 20 wt % MgO) most probably due to olivine accumulation and, thus, is already relatively primitive and does not require fractionation correction. Moreover, phaneritic and crystal-rich samples may not represent the true liquidus composition of Juan Fernandez magmas.

Juan Fernandez samples span a narrow range of wt% FeO* = 8.91-13.3, and wt% $Na_2O$ = 1.54 - 4.74 (Fig. 3.2). Of the lava groups, group II has the highest wt% $Na_2O$ with a range of 2.72 - 4.74, and high wt% FeO* values as well, suggesting they were produced by relatively smaller degree at $\sim$ higher pressure of melting. Group I on average has a large range that includes the lowest wt% $Na_2O$ values and low wt% FeO*, whereas group III has uniform and intermediate wt% $Na_2O$ and higher wt% FeO* values. These suggest groups I and III were produced by moderate degrees of melting at low to moderate pressures. Although these results are qualitative because of the aforementioned caveats, they have some significance because they are consistent with the following trace element and modeling results.

## 3.2 Incompatible Trace Element Variation

Juan Fernandez lava groups show sub-parallel, incompatible trace element-enriched concentration patterns that suggest a common, fairly homogeneous source (Figs. 2.1 and 2.2). In detail, group II is the most enriched and group I is slightly more enriched than group III. The overlapping incompatible-element enrichments in group I R. Crusoe and group III A. Selkirk basalts suggest comparable degrees

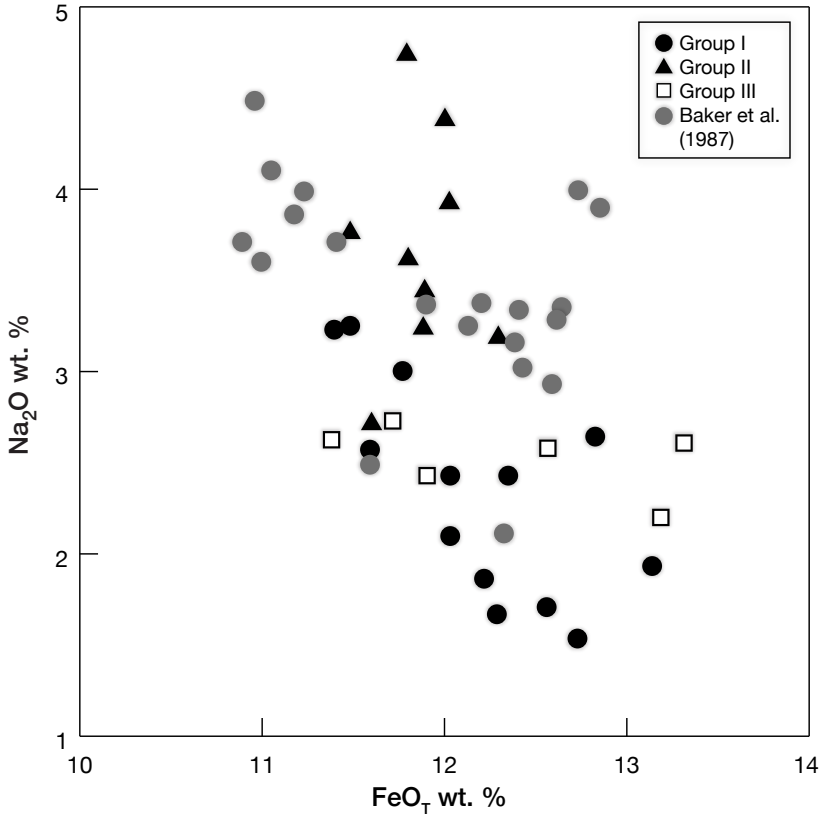


**Figure 3.2**: Diagram showing $Na_2O$ wt. % versus FeO* ($FeO_{Total}$) wt. % for Juan Fernandez lavas to illustrate the relative pressure and degree of partial melting concept of *Klein and Langmuir* [1987]. Major element values for Juan Fernandez lavas are from *Farley et al.* [1993]; values from previous study of *Baker et al.* [1987] are shown in grey.

of partial melting for the shield-building stage of both islands. In contrast, the more elevated pattern of group II basanites is consistent with smaller degree of partial melting.

It is noteworthy that *Natland* [2003] proposed that some of the elevated concentrations of incompatible elements in Juan Fernandez olivine-rich tholeiites result from mixing between primitive (i.e., high-MgO) and highly differentiated (low-MgO) lavas. *Natland* [2003] further asserted that post-shield basanites on R. Crusoe do contain xenocrysts of mantle mineral phases spinel, olivine, clinopyroxene, and orthopyroxenes. On average, the incompatible element-enriched group II basanites have a narrow, intermediate range of MgO relative to groups I and III (Fig. 3.1). Furthermore, the majority of olivine phenocrysts in the samples are euhedral and do not indicate a history of convective movements [*Farley*, 1991]. Hence, it would require some pleading to explain why group II basanites, which have intermediate MgO, have the highest incompatible trace element concentration. A simpler, unified explanation is needed to explain both the trace element and major element variations of Juan Fernandez lavas.

Overall, the similarity of REE and highly incompatible element concentration patterns of groups I and III basalts suggests an origin from a common mantle source for both R. Crusoe and A. Selkirk shield-building lavas. Between the two basalt groups, group III is less enriched in highly incompatible elements, suggesting they were produced by ∼higher degree of partial melting than group I. The steep REE patterns and largest enrichments in highly incompatible elements suggest group II was produced by a smallest degree of partial melting of the same mantle source. Significantly, a similar difference in incompatible trace element variations exist between current Galápagos volcanoes and their apparent track along the Cocos Ridge and this has also been interpreted as due to differences in extent of partial

melting of a common source [*Hoernle et al.*, 2000]. The contrasting variations in incompatible elements between the Cocos track profile and the Galápagos Islands must also primarily reflect differences in extent of melting rather than source variation, because the compositional structure of the plume appears to have remained constant over the past 14 m.y.

The incompatible trace element variations of Juan Fernandez lavas when plotted in the process identification diagrams of *Minster and Allègre* [1978] and *Feigenson et al.* [1983] show that group II was produced by smaller degree of partial melting of the common source whereas groups I and III were produced by higher degrees (Fig. 3.3), consistent with the qualitative results from major element modeling data (Fig. 3.2). Moreover, differences in the degree of partial melting between groups III and I is apparent in Nb/Zr vs. Nb and Ba/Zr vs. Ba diagrams; the former appears to have undergone a slightly larger degree of partial melting than the latter.

In detail, model calculations using the variation of La/Yb vs. La (ppm) (Fig. 3.3A) illustrate that the trace element characteristics of Juan Fernandez lavas can be produced through variable degrees of partial melting of a garnet peridotite source. The model uses the *Shaw* [1970] modal batch melting equation, a source with 60% olivine, 21% orthopyroxene, 8% clinopyroxene, and 11% garnet (i.e., garnet peridotite) containing 2.1 ppm La and 1.1 ppm Yb [*Frey*, 1980], and bulk partition coefficients $D_{La} = 0.00538$ and $D_{Yb} = 0.82425$ for a garnet peridotite-basaltic melt system [*Johnson*, 1998]. Results show that group I and III basalts plot along the batch melting curve for the garnet peridotite at ∼12 - 35% partial melting, with group III at a ∼higher % melting than group I on average. On the other hand, group II basanites that have the highest La and La/Yb values fall to the right of the batch melting line, indicating La enrichment with fractional crystallization.

Nevertheless, the intersection between group II fractional crystallization array and garnet peridotite melting curve indicates that it was produced at the lowest degree of partial melting (<10%). Thus, model calculations indicate that the shield-building groups I and III Juan Fernandez lavas were produced by relatively high degree of partial melting whereas the post-shield group II basanites by smaller degree. The latter also exhibits the largest effect of fractional crystallization. These processes could explain the overall lower and overlapping incompatible trace element concentrations of groups I and III lavas and the higher or more fractionated incompatible trace element concentrations of group II (Figs. 2.1 and 2.2). The relatively high degree of fractional crystallization of group III is also consistent with its intermediate MgO values (Fig. 3.1).

In summary, the major and trace element variations of Juan Fernandez lavas can be explained through variations of degree and, to a certain extent, pressure (depth) of partial melting of a common mantle source characterized by a fairly limited Sr, Nd and Pb isotopic variation. The geochemistry of group II can be modeled as the result of small degrees of partial melting (+ fractional crystallization) whereas groups I and III represent ∼larger degree partial melts. This simple model is based on the assumption that all lavas were produced by equilibrium batch partial melting [*Shaw*, 1970] of a ∼common mantle source that exhibits limited variations in isotopic composition (Figs. 2.3 and 2.4).

## 3.3 The Sr-Nd-Pb composition of the Juan Fernandez mantle source

Despite the relatively limited range in values compared to other OIB groups [this study; *Gerlach et al.*, 1986; *Farley et al.*, 1993], the Sr, Nd and Pb isotopic

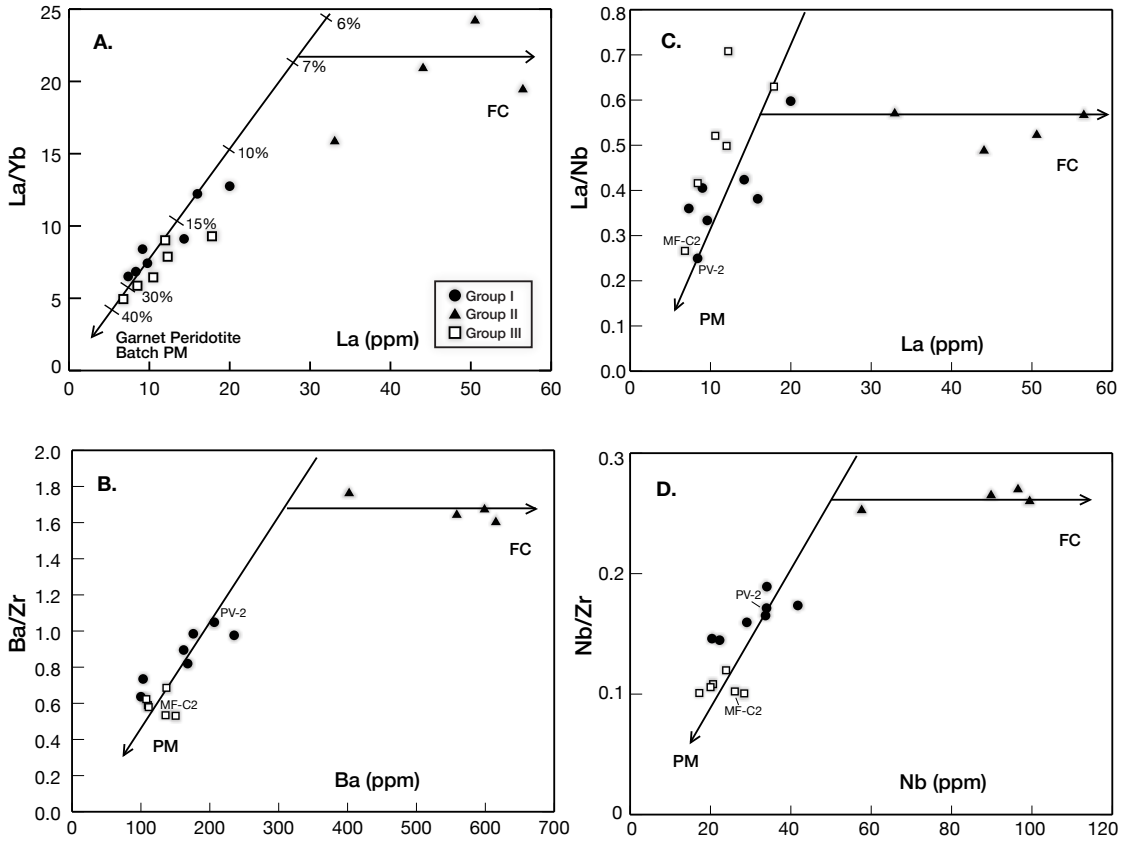


**Figure 3.3**: Magmatic process identification diagrams after *Allègre and Minster* [1978]; see also, *Minster and Allègre* [1978]; *Feigenson et al.* [1983] for Juan Fernandez lavas. PM represents equilibrium batch partial melting and FC represents fractional crystallization. **A.** La/Yb vs. La (ppm) modeled by partial melting curve [*Shaw*, 1970], with tick marks indicating percentage of melt. A garnet peridotite source with 60% olivine, 21% orthopyroxene, 8% clinopyroxene, and 11% garnet and containing 2.1 ppm La and 1.1 ppm Yb as well as bulk partition coefficients $D_{La} = 0.00538$, $D_{Yb} = 0.82450$ were used in the modeling. Results show that groups III and I were generated at relatively high (> 10% - 35%) degree of partial melting although on average group III was at higher degree (>15%) than group I (<30%). Group II was produced at the lowest degree of partial melting. **B.** Ba/Zr vs. Ba (ppm) and **D.** Nb/Zr vs. Nb (ppm) consistent with the modeling results. In summary, groups II, I and III were produced by increasing degree of partial melting and fractional crystallization was also important in producing group II basanites.

ratios of Juan Fernandez lavas show a slight though distinct variation in the isotopic composition of their mantle source [see also *Gerlach et al.*, 1986]. The new Pb isotopic analyses when combined with previously available Sr and Nd isotopic data systematically identify two geochemically enriched mantle source components. One component is on average more enriched than the other, with higher $^{87}Sr/^{86}Sr$, lower $^{143}Nd/^{144}Nd$ and more radiogenic $^{206}Pb/^{204}Pb$ ratios. This is represented by group I lavas. Group II greatly overlaps with group I, but generally occupies the least radiogenic end of the array. The less enriched component is represented by group III and has lower $^{87}Sr/^{86}Sr$, higher $^{143}Nd/^{144}Nd$ and less radiogenic $^{206}Pb/^{204}Pb$ ratios. Group III has overlapping though slightly higher $^{143}Nd/^{144}Nd$ and $^{87}Sr/^{86}Sr$ than group II.

From the Sr-Nd-Pb isotopic viewpoint, the long-lived radiogenic isotopic ratios of Juan Fernandez lie near the FOZO. In terms of Sr and Nd isotopes, FOZO has had a long time-integrated history of depletion because it has higher $^{143}Nd/^{144}Nd$ and lower $^{87}Sr/^{86}Sr$ than the bulk silicate Earth [e.g., *Hofmann*, 2003; *Stracke et al.*, 2005; *White*, 2010; *Castillo*, 2015]. Although the isotopically ∼depleted FOZO source of Juan Fernandez is enriched in incompatible trace elements and, in terms of Pb isotopes, projects toward the proposed HIMU mantle end-member or, simply, FOZO is a 'young HIMU' [*Thirlwall*, 1997; *Stracke et al.*, 2005; *Castillo*, 2015]. However, the mantle source of Juan Fernandez also contains a relatively less-enriched component typical of the higher $^{143}Nd/^{144}Nd$ and lower $^{206}Pb/^{204}Pb$ ratios of the proposed EM1 end-member. Notably, *Gerlach et al.* [1986] have suggested a similar isotopic characterization of the mantle source of Juan Fernandez; however, their notion was deduced from the combined isotopic ranges of Juan Fernandez, San Felix and San Ambrosio islands that all lie on the Nazca plate. *Gerlach et al.* [1986] proposed that these islands define an array of

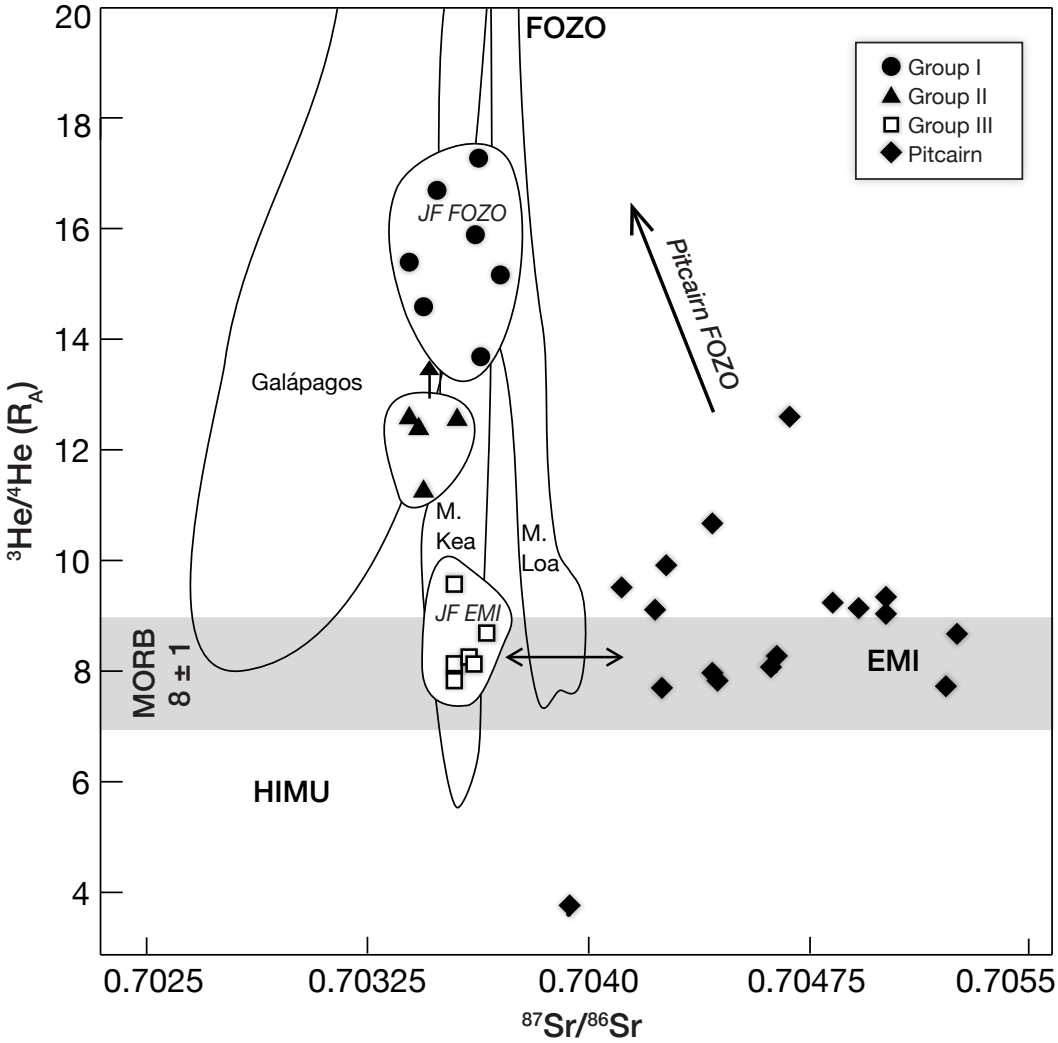


**Figure 3.4**: $^{3}He/^{4}He$ ($R_A$) versus $^{87}Sr/^{86}Sr$ for Juan Fernandez (this study) and Pitcairn [*Garapić et al.*, 2015; *Honda and Woodhead*, 2005]. Fields for Mauna Kea (M. Kea), Mauna Loa (M. Loa) and Galápagos) (from GEOROC database - http://georoc.mpch-mainz.gwdg.de/georoc/) are shown for reference. Note that like Juan Fernandez, the Hawaiian mantle plume has an EM1-like signature [*Garapić et al.*, 2015].

low $^{143}Nd/^{144}Nd$ for given $^{87}Sr/^{86}Sr$, which they termed the 'LoNd' mantle array; the array is also characterized by ∼high $^{206}Pb/^{204}Pb$ ratios. In their scheme, the spread of the isotopic ratios in the LoNd array is also from a mixture of EM1 and (young) HIMU mantle end-members. In this study, the new isotopic data for Juan Fernandez project from EM1 end-member toward FOZO component (Fig. 3.4) similar to the interpretation of *Gerlach et al.* [1986].

## 3.4 The geochemistry of Juan Fernandez Islands compared to some Pacific island chains

The observed geochemical evolution of Juan Fernandez Islands resembles that of Jasper Seamount of the Fieberling-Guadalupe Seamount Trail, which displays many aspects of Hawaiian evolution despite its small size [*Konter et al.*, 2009]. The seamount demonstrates three individual stages that represent decreasing degrees of partial melting with time. In Jasper, the most voluminous shield building stage was followed by the younger and substantially less voluminous flank series that is comparatively depleted in Sr and Nd isotopic ratios and more enriched in incompatible trace elements [*Konter et al.*, 2009]. The combined R. Crusoe and A. Selkirk data are similar to the first two stages of Jasper evolution. The details of the geochemistry of the youngest Friday and Domingo seamounts are not yet well established [*Farley*, 1991; *Farley et al.*, 1993; *Devey et al.*, 2000] and, thus, it is difficult to relate these to the last stage of the geochemical evolution of Jasper Seamount [cf., *Konter et al.*, 2009].

The geology of R. Crusoe also bears gross similarities to that of Tahaa, the largest of the Society Islands [*White and Duncan*, 1996]. Tahaa has an age range of 2.3 Ma with a volcanic hiatus between the shield building and post-erosional stages

of 1.2 Ma. Thus, the time-scale of its compositional variation is less than 1 m.y. Based on available age data, a similar hiatus in volcanic activity is exhibited by lavas of R. Crusoe. The latter phase in Tahaa has a less-enriched isotopic signature compared to the earlier shield building stage, again similar to the shield  post-shield isotopic relationship in R. Crusoe. Based on observations at Tahaa, *White and Duncan* [1996] proposed that Society Islands were created by two heterogeneous mantle end-members: a high $^{87}Sr/^{86}Sr$ component that is the core of the plume, and a low $^{87}Sr/^{86}Sr$ component that is the 'sheath' of the plume, which was created as the plume entrained the ambient upper mantle during ascent.

*Chauvel et al.* [2012] found that the tholeiites on the island of Ua Huka, representing the shield-building phase of plume magmatism in the Marquesas archipelago, have high $^{87}Sr/^{86}Sr$ whereas the post-shield basanites have lower $^{87}Sr/^{86}Sr$. This isotopic pattern parallels the high $^{87}Sr/^{86}Sr$ of group II shield-building tholeiites and lower $^{87}Sr/^{86}Sr$ of group I post-shield basanites in R. Crusoe (Fig. 2.3). Significantly, Chauvel also observed a possible relationship between degree of partial melting of the source and strength of its original isotope diversity. Results of their study indicate that isotopic variations in OIB are controlled by source composition that changes through time. Moreover, trace element plus isotopic variation, to a certain extent, depends on the degree of partial melting because different degrees of partial melting can sample distinct mantle sources as clearly seen in off-axis seamount and fossil spreading center lavas [e.g., *Zindler et al.*, 1984; *Graham et al.*, 1988; *Castillo et al.*, 2010; *Tian et al.*, 2011].

In addition to the above similarities to other linear volcanic chains, the $\delta^{18}O$ values of Juan Fernandez as a whole are relatively homogeneous and similar to those of MORB and other OIB - particularly those with high-$^{3}He/^{4}He$ ratios [*Eiler et al.*, 1997]. Moreover, calculated values of Nb/Nb* anomalies [*McDonough*, 1991;

*Jackson et al.*, 2008] of Juan Fernandez lavas range from 1.36-2.87, with A. Selkirk group III basalts having the lowest value. However, on average, these anomalies are higher than most OIB. Calculated Ta/Ta* values range from 1.48-3.09; group III again has the lowest Ta/Ta* value. Calculated Ti/Ti* values range from 0.74-2.07 and are highest in group III. In other words, Juan Fernandez exhibits TITAN positive anomaly, again similar to some high-$^3$He/$^4$He OIB [*Jackson et al.*, 2008]. However, although Juan Fernandez lavas exhibit positive TITAN anomalies, there is no correlation between the size of the TITAN anomaly and $^3$He/$^4$He variation [cf. *Jackson et al.*, 2008, see Fig. 3.6], as also clearly pointed out by *Peters and Day* [2014]. Finally, similar to other high-$^3$He/$^4$He OIB in the southern hemisphere, Juan Fernandez belongs to the high-$^3$He/$^4$He group that is claimed to be originating from a southern high-$^3$He/$^4$He reservoir (FOZO-A, Austral); this is in contrast to the high-$^3$He/$^4$He OIB group in the northern hemisphere, which originates from the northern high-$^3$He/$^4$He reservoir (FOZO-B, Boreal; for details, see Figure 2 of *Jackson et al.*, 2007).

## 3.5 The volcanologic evolution of Juan Fernandez islands

Using field observations and petrographic, major-trace element, plus Sr-Nd-Pb isotopic data (*Gerlach et al.*, 1986; *Baker et al.*, 1987; *Farley*, 1991; *Farley et al.*, 1993; *Natland*, 2003, this study) and the aforementioned geologic similarities with other oceanic islands, the following model for the geologic evolution of Juan Fernandez islands is proposed (Fig. 3.5).

The pre-shield building stage magmatism (Fig. 3.5A) is still not well understood, but results of volcanic island investigations suggest that it is a heterogeneous

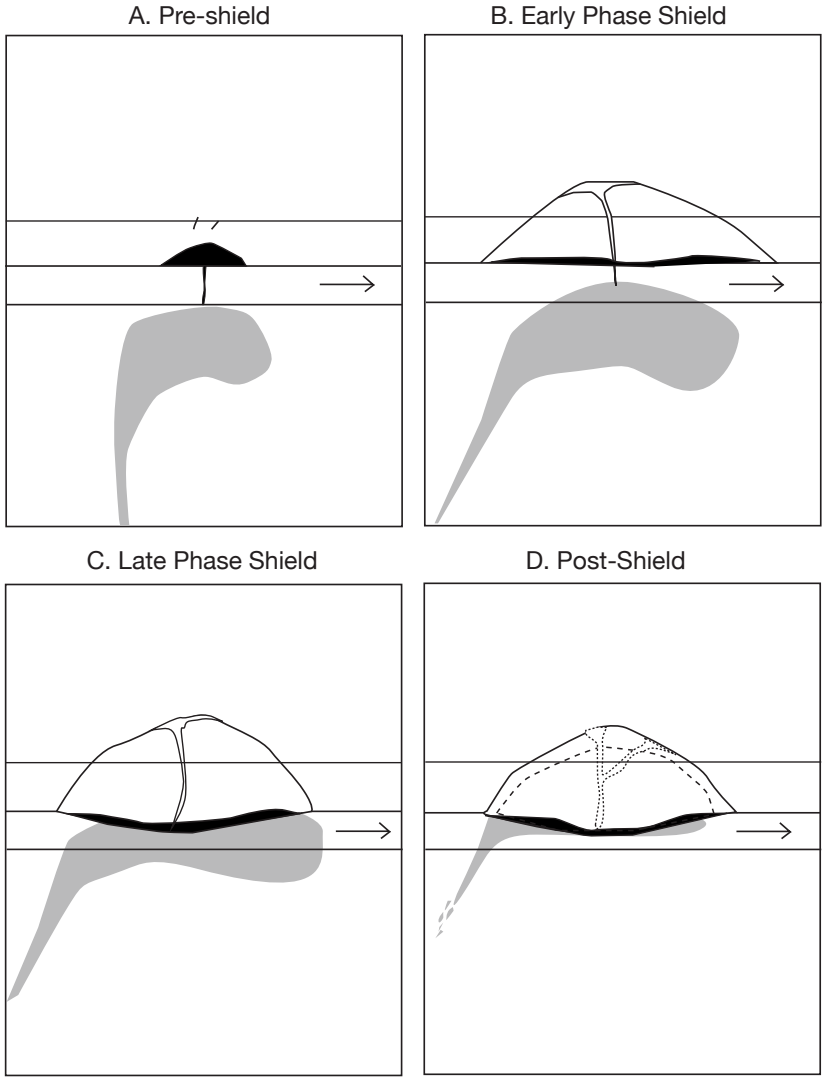


**Figure 3.5**: Proposed stages of the volcanologic evolution of Juan Fernandez Islands. **A**. Pre-shield, **B**. Early Phase shield, **C**. Late Phase shield, **D**. Post-Shield. See text for discussion.

mixture of lavas that precedes the arrival of the main body of the upwelling mantle plume. These produce the submarine, or emerging stage of volcanoes. *Devey et al.* [2000] reported that magmas from the submarine volcanoes, Friday, and the more westerly Domingo, are highly alkaline. These are characterized by variable, but generally small degrees of partial melting of the plume source. Thus, lavas at this stage have a variable composition because the core component of plume has not yet impinged the lithosphere. This stage would be represented by inaccessible, not yet sampled, lowermost structures of both R. Crusoe and A. Selkirk, and of Domingo and Friday seamounts.

The early shield-building stage (Fig. 3.5B) is best represented by group III basalts. Constituting the bulk of A. Selkirk, group III basalts are produced by slightly larger degrees of partial melting, relative to the more enriched group I late shield-building type. This stage represents partial melting of the less enriched component, or 'core' of the mantle plume. This is compatible with a previous proposal that the low Ba/Zr ratio A. Selkirk relative to group I/II reflects group III tapping a somewhat different source from R. Crusoe [*Farley*, 1991]. At this stage, the mantle plume yields more EM1-like magmas. Lavas are mainly tholeiitic to transitional to alkalic basalts that are 'relatively depleted' in incompatible elements and isotopic ratios. They also have a MORB-like $^{3}He/^{4}He$ ratio of $8\pm1$ $R_A$, which is the characteristic He isotopic signature of EM1 [*Honda and Woodhead*, 2005; *Garapić et al.*, 2015].

The late phase of shield-building stage (Fig. 3.5C) is characterized by R. Crusoe group I basalts. *Baker et al.* [1987] proposed their central group consists o1f lavas representing an earlier phase of activity relative to peripheral group. Thus, the central group of *Baker et al.* [1987] and the olivine tholeiites of group I found at Puerto Vaqueria [*Farley et al.*, 1993] best characterize this shield-building phase,

and have the highest $^3He/^4He$ ratios on the entire chain. Specific to Juan Fernandez, this is the late phase of sampling the Juan Fernandez plume and, thus, yields the FOZO or young HIMU signature with high-$^3He/^4He$ ratios.

The post-shield or post-erosional stage (Fig. 3.5D) is evident by late capping and minor intrusives and represented by group II basanites in R. Crusoe. These are small degree partial melts coming from the tail end of the mantle plume. They occur as parasitic cones and dikes that cross-cut the underlying shield lavas [*Baker et al.*, 1987]. These lavas consist of basanites and are more Si-undersaturated compared to shield-building lavas. Small volume alkalic melts that intrude pre-existing lava formations are more susceptible to alteration or crustal modification, like the slightly higher $\delta^{18}O$ signature of the basanites observed by *Eiler et al.* [1997]. Isotopically, they resemble FOZO compositions.

As discussed above, results of this study suggest that the post-shield group II basanites were also derived $\sim$1 m.y. later from the same mantle plume that upwelled from below and underplated the lithosphere during the transition from shield to post-shield stage (Fig. 3.5D). This notion is clearly supported by field observations showing that basanites are smaller in volume and consist mainly of parasitic cones and dikes intruding basaltic flows, petrologic evolution from parental melt to basanite, as well as major and trace element models (Figs. 3.2 and 3.3).

## 3.6 Implications for the origin of the high-$^3He/^4He$ signature of Juan Fernandez lavas

A remarkable feature of Juan Fernandez lavas is their $^3He/^4He$ ratios range from 7.8-18.0 $R_A$, spanning the normal ratio of MORB [$8 \pm 1$ $R_A$ *Graham*, 2002] and the higher ratios of many OIB [>9 up to 50 $R_A$ *Stuart et al.*, 2003; *Kurz et al.*, 1983],

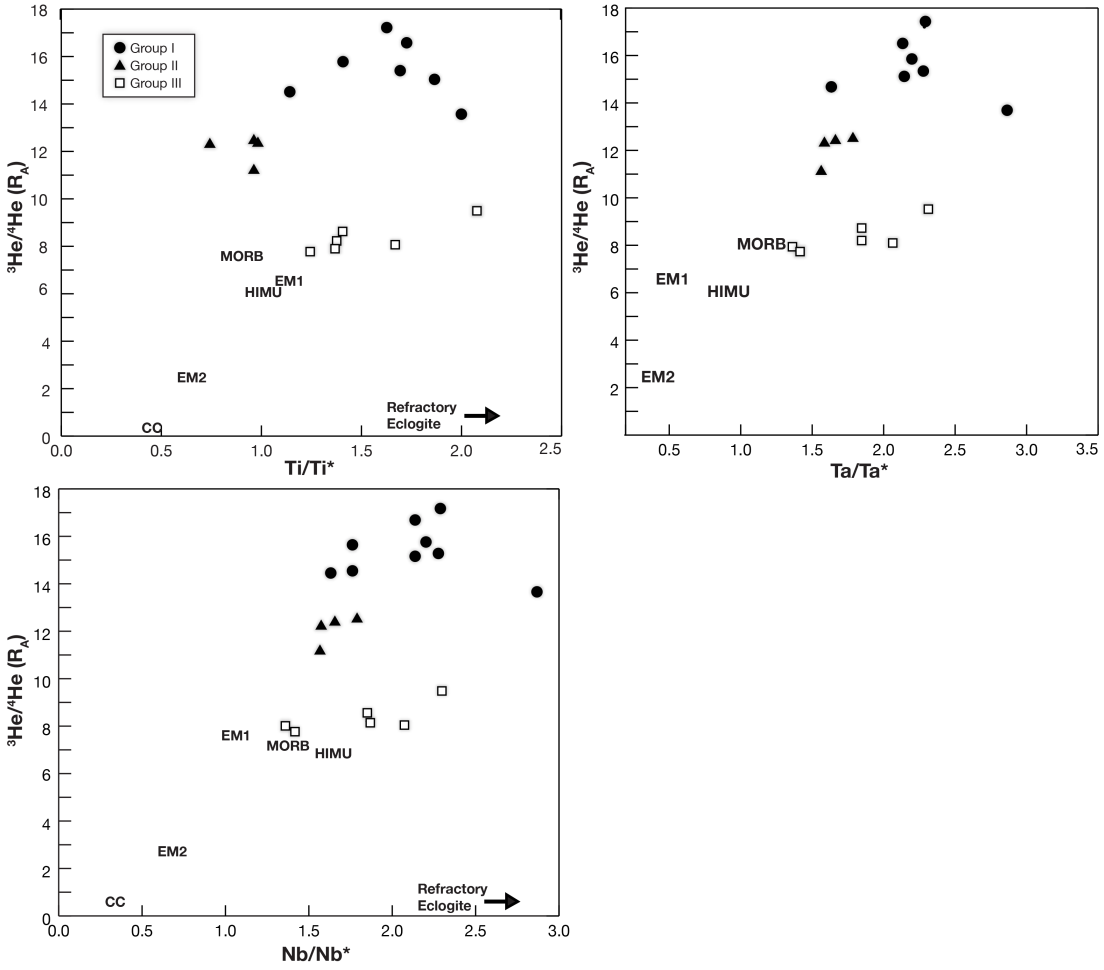


**Figure 3.6**: Relationships between TITAN (Ti/Ti*, Ta/Ta*, and Nb/Nb*) anomalies and $^3He/^4He$ ($R_A$) in Juan Fernandez lavas. TITAN calculations, refractory eclogite, and end-member compositions are from *McDonough* [1991]; *Jackson et al.* [2008]. Nb, Ti and Ta anomalies were calculated using data normalized to primitive mantle values of *Sun and McDonough* [1989].

but have a fairly limited range of Sr-Nd-Pb isotopic ratios. This lack of correlation or apparent decoupling between $^{3}He/^{4}He$ ratios and Sr, Nd and Pb isotope tracers in Juan Fernandez lavas contrasts to the $^{3}He/^{4}He$ and isotope correlations displayed by some other high-$^{3}He/^{4}He$ OIB (e.g., Hawaii, Iceland, Galápagos) that can be modeled or interpreted less equivocally [e.g., *Hilton et al.*, 1999]. Thus, one of the major conclusions of this study is that the true origin of the high-$^{3}He/^{4}He$ signature of Juan Fernandez can only be constrained by combining results of detailed He isotopic [*Farley*, 1991; *Farley et al.*, 1993], petrologic investigations (e.g., this study), and of future complementary investigations particularly of other noble gases (e.g., Ar, Ne) and fluids [e.g., $CO_2$, $H_2O$; *Hilton et al.*, 1997, 2000].

### 3.6.1 The MORB-like $^{3}He/^{4}He$ of group III lavas

The present study, however, stresses a number of key geochemical results that must be taken into account when results of such complementary investigations to explain the true source of high-$^{3}He/^{4}He$ signature of OIB become available. The first set of results bear on the occurrence of MORB-like $^{3}He/^{4}He$ ($8 \pm 1$ $R_A$) in Juan Fernandez. This was previously explained as partly due to involvement of the asthenospheric source of MORB (or DMM) in the production of Juan Fernandez lavas [*Farley*, 1991; *Farley et al.*, 1993]. However, major and trace element and Sr-Nd-Pb isotopic data do not indicate any involvement of DMM. In particular, the low to moderate $^{206}Pb/^{204}Pb$ high $^{208}Pb/^{204}Pb$ for a given $^{206}Pb/^{204}Pb$ (i.e. plotting above the NHRL- Fig. 2.4) and slightly high $^{87}Sr/^{86}Sr$ and low $^{143}Nd/^{144}Nd$ (Fig. 2.3) in Juan Fernandez group III lavas (with $^{3}He/^{4}He = 8$ $R_A$) approach the EM1 characteristics observed in Pitcairn and Hawaii [*Garapić et al.*, 2015] as well as Kergulen [*Silva et al.*, 2013] lava suites. These isotopic features reflect an ancient geochemical enrichment clearly distinct frm the ancient geochemical

depletion experienced by DMM [*Hofmann*, 2003; *White*, 2010]. Thus, a simple derivation of Juan Fernandez $^3He/^4He$ with 8 $R_A$ is highly inconsistent with the bulk of available data.

Furthermore, the isotopic composition of Juan Fernandez basalts show no evidence of continental lithospheric contamination. Unlike the continental lithosphere, all groups are enriched in Nb and Ta relative to primitive mantle (Figs. 2.2, 3.6). All groups also show higher $^3He/^4He$ than subcontinental lithospheric mantle ($\sim$6.1$R_A$, *Gautheron and Moreira*, 2002), and group III lavas with $^3He/^4He$ = 8 $R_A$ show the lowest radiogenic Pb isotope signatures. Thus, the trace element and isotopic characteristics of Juan Fernandez lavas with low-$^3He/^4He\sim$8 $R_A$ most likely reflect the nature of their original mantle source, and do not show involvement of DMM or lithospheric contamination.

Instead, results of this study show that the Juan Fernandez plume source consists of FOZO, the common source of high-$^3He/^4He$ (>9 $R_A$) OIB [e.g., *Hilton et al.*, 1997; *Hanan and Graham*, 1996; *Castillo*, 2015], and an EM1 end-member, which has recently been described as having a MORB-like $^3He/^4He$ of 8$\pm$1 $R_A$ [*Honda and Woodhead*, 2005; *Garapić et al.*, 2015]. That is, group III A. Selkirk basalts have the EM1 end-member $^3He/^4He$ which is indistinguishable from that of MORB (Fig. 3.4). Thus, sampling these two mantle components through sequential and variable degrees (Figs. 3.2, 3.3A-D, and 3.5) of partial melting explain the observed MORB-like (EM-1) to high-$^3He/^4He$ OIB-like (FOZO) He and limited Sr-Nd-Pb isotopic characteristics of Juan Fernandez. In contrast, almost all high-$^3He/^4He$ OIB, such as those in Hawaii and the Galápagos, show continuous or apparent mixing trends between high and lower $^3He/^4He$ values. The difference makes the task of comparing the petrogenesis of Juan Fernandez lavas more difficult than those of the other high-$^3He/^4He$ OIB.

### 3.6.2 The difference in $^3He/^4He$ between group I and group II lavas

In detail, *Farley et al.* [1993] proposed binary mixing between a high-$^3He/^4He$ primitive, 'Loihi-type', undegassed, and geochemically enriched reservoir, representing the Juan Fernandez plume, and DMM primarily to explain the lower $^3He/^4He$ range of group II basanites compared to that of group I basalts in a fashion similar to several Hawaiian volcanoes [*Kurz et al.*, 1983]. As discussed above, results of this study indicate that the DMM is not involved in the generation of Juan Fernandez lavas. Instead, results show that the post-shield group II basanites were also derived ∼1 m.y. later from the same mantle plume that upwelled from below and underplated the lithosphere during the transition from shield to post-shield stage (Fig. 3.5C-D). This notion is clearly supported by field observations showing that basanites are smaller in volume and consist mainly of parasitic cones and dikes intruding basaltic flows, petrologic evolution from basalt to basanite, major and trace element models (Figs. 3.2 and 3.3A-D), and most important, the modest range in Sr-Nd and the completely overlapping Pb isotopic ratios between groups I and II indicate a common plume source (Figs. 2.3 and 2.4).

Notably, Juan Fernandez lavas as a whole are geochemically enriched, and thus, contain high concentrations of incompatible trace elements such as Th and U. Consequently, the high U and Th can lower the $^3He/^4He$ ratio in group I basalts to group II basanites while maintaining a constant Sr-Nd-Pb isotopic composition in both groups during the 1 m.y. transition or hiatus from shield to post-shield (Fig. 3.5C-D). Of course, this can only occur if there is sufficient time to grow enough $^4He$ to lower $^3He/^4He$ in a closed system environment. However, an open system environment most likely developed through degassing of Juan Fernandez

volcanoes during the transition or hiatus from shield to post-shield stages and degassing can lower the concentration of He with the original $^3He/^4He$ component [*Hilton et al.*, 1997, 2000].

*Graham et al.* [1987] introduced an equation that may illustrate how $^3He/^4He$ decreased from group I (>13 $R_A$) to group II (11-12.5 $R_A$) during the 1 m.y. transition from late shield to post-shield building stage. The amount of radiogenic ingrowth, $^4He^*$, produced from group I alkali basalt can be calculated using the equation:

$$^4He^* = 2.80 \times 10^{-8}\{[U](4.35 + Th/U)\}T(cm^3\ STP\ g^{-1}) \qquad (3.1)$$

Table 3.1 lists the results of this modeling, where the average concentrations of group I alkali basalt $^3He$ (column 1) and $^4He$ (column 2) are combined with the average U+Th concentrations of group II basanites to generate a total amount of $^4He$ * produced (column 3). *Graham et al.* [1987] suggested that 1-10% of this total ingrwoth would be retained. Thus, the new $^3He/^4He$ ($R_A$) for a particular basanite (column 4) uses a range of percentages (column 5) to represent the small % of $^4He^*$ that is finally retained.

**Table 3.1**: Recalculated $^3He/^4He$ ($R/R_A$) ratios from group I/II chemical analyses

| $^3$**He (cc/g)** | $[He]_{AB}$ **cc/g** | $[He]^*_{BSN}$ **cc/g** | $^3$**He/**$^4$**He (R/R$_a$)** | **%** |
|---|---|---|---|---|
| $4.91\times10^{-13}$ | $2.21\times10^{-8}$ | $3.75\times10^{-7}$ | *12.7* | 1.5 |
| $4.91\times10^{-13}$ | $2.21\times10^{-8}$ | $3.75\times10^{-7}$ | *11.9* | 2.0 |
| $4.91\times10^{-13}$ | $2.21\times10^{-}8$ | $3.75\times10^{-7}$ | *11.2* | 2.5 |

AB = Alkali Basalt (group I), BSN = Basanite (group II).
Italicized numbers are in target range of group II $^3He/^4He$ = 10.9 - 12.8 $R_A$. $^3He$ and $^4He$ measurements from *Farley et al.* [1993].

Resulting calculations show the small percentage of $^4He^*$ produced by the

average alkali basalt U+Th composition can substantially lower the $^3He/^4He$ of a later basanite group with the same source. U and Th are generally excluded from olivine phenocrysts as they reside in the rock groundmass, and outgassing of $^4He^*$ as it is being produced can result in only 0.05 - 3.5% of ingrowth retained by basanite olivine phenocrysts. This conservative estimate is highly consistent with the proposal by *Graham et al.* [1987] that only 1-10% of $^4He^*$ ends up enclosed in phenocrystic olivines. Therefore, it is theoretically possible to produce the observed $^3He/^4He$ of the basanites in a fractionating magma very similar to the source of group I alkali basalts (similar Sr, Nd and Pb isotopic ratios) within 1 million years. To a first order, enclosing a mere <4% of $^4He^*$ in such a magma can explain the observed lower group II $^3He/^4He$ than group I lavas, assuming all $^3He$ is inherited.

If group I $^3He/^4He$ can decrease to the observed range of group II $^3He/^4He$, group II $^3He/^4He$ may simply be the late shield-building group I, but with a present-day $^3He/^4He$ ratio that includes radiogenic ingrowth of $^4He^*$ during the 1 m.y. transition between stages.

### 3.6.3 The nature of $^3He/^4He$ in Juan Fernandez lavas

Although the occurrence of different groups of lavas with distinct trace element and particularly $^3He/^4He$ signatures precludes a clear binary mixing relationship between discrete mantle endmember sources (e.g. Figs. 1.3, 2.1, 2.2, 3.4), binary mixing between magmas is apparent in a couple samples. Specifically, it was noted earlier that PV-2 was originally classified as group II basanites in R. Crusoe, but its Sr-Nd-Pb ratios are most similar to those of the group I basalts. The transitional characteristics of this sample is most probably due to mixing of basalt and basanite magmas produced during the transition from the climax of the late shield-building stage to the post-shield stage. Not surprisingly, sample PV-2

basanitoid has $^{3}He/^{4}He = 13.6\ R_A$, transitional between groups I and II. On the other hand, sample MF-C2, the only sample from A. Selkirk which has a $^{3}He/^{4}He = 9.5\ R_A$, a value higher than MORB range, was collected from the island's summit. It most likely represents the youngest eruptive in A. Selkirk that was transitioning to a late R. Crusoe-type stage, whence the higher $^{3}He/^{4}He$ component of the plume source was sampled.

Thus, the new results do not support a need for involvement of any asthenospheric material in the production of group II R. Crusoe lavas, as proposed by *Farley et al.* [1993].

The distinct, though limited Sr-Nd-Pb heterogeneity in the mantle plume source of Juan Fernandez lavas (Figs. 2.3 and 2.4) is also observed in the plume source of French Polynesian OIB [e.g., *Chauvel et al.*, 1992]. Results of this study also imply heterogeneous distribution of volatiles in the mantle plume, as deduced from the difference in the $^{3}He/^{4}He$ signatures of R. Crusoe and A. Selkirk shield building lavas [*Farley et al.*, 1993]). Moreover, sample MF-C2, the only sample from A. Selkirk that has $^{3}He/^{4}He$ higher than the MORB range, at $9.5\ R_A$, was collected from the islands summit. Hence, it most likely represents the youngest eruptive in A. Selkirk that was transitioning to the R. Crusoe stage, whence the higher $^{3}He/^{4}He$ component of the plume source was being sampled.

Finally, the overall similarity of the $^{143}Nd/^{144}Nd$ ratios of the olivines and host rocks (Table 2.1) suggests that the $^{143}Nd/^{144}Nd$ values preserved by the olivines are in equilibrium with those in their respective host magmas. That is, the olivine phenocrysts equilibrated with the last drop of melts in Juan Fernandez, despite their complex crystallization histories as clearly evidenced in the petrography of these olivines [*Natland*, 2003]. Neodymium, similar to He, occurs in trace amounts in olivine as its distribution coefficient in olivine is very low [$K_d = 0.006$; *Rollinson*,

1993]. Altogether, these results suggest that there is a small but distinct, inherent compositional heterogeneity in the source of Juan Fernandez lavas and, thus, do not support the idea that the decoupling between $^{3}He/^{4}He$ and Sr, Nd and Pb isotope ratios can be explained through relatively shallow level disequilibrium reactions between olivine and melts [*Natland*, 2003]. Instead, results suggest that the differences in $^{3}He/^{4}He$ and $^{143}Nd/^{144}Nd$ preserved by the olivines represent distinct, inherent compositional heterogeneity of the mantle plume source of Juan Fernandez lavas.

# 4 Conclusions

This study presents new trace element and Sr, Nd, and Pb isotopic analyses of Juan Fernandez lavas to further constrain their petrogenesis and mantle source composition. The new analyses are consistent with previous results showing that the outcrops in R. Crusoe consist of groups I and II basalts and basanites, respectively, whereas those in A. Selkirk consist of group III basalts. Variations in major and trace element composition of the lavas are mainly controlled by differences in degrees of partial melting of a common source. Overall, major and trace element data and modeling suggest that A. Selkirk group III basalts were produced by the largest degree of melting at moderately low pressure, followed by R. Crusoe group II basalts. R. Crusoe group II basanites were produced by the smallest degree of partial melting. Fractional crystallization accounts for some of the compositional variations of the rock groups, particularly those in the R. Crusoe group II basanites.

The new data confirm the limited range of Sr, Nd and Pb isotopic ratios of Juan Fernandez lavas despite their range of (7.8 - 18.0 $R_A$) of $^3He/^4He$ values. Similar to the major and trace element result, the limited isotopic range indicates that the parental magmas for Juan Fernandez lavas are derived from a common, mantle plume source that resides in the FOZO region inside the Sr-Nd-Pb isotopic space. A small but distinct compositional variability exists within this source. Melts with an EM-1-like flavor ($^3He/^4He = 8$ $R_A$) are preferentially sampled by A. Selkirk

whereas melts from FOZO ($^3He/^4He > 9$ $R_A$) with young HIMU isotopic affinity are preferentially sampled by R. Crusoe melts. Thus, the range of $^3He/^4He$ (8-18 $R_A$) simply represents EM1 and FOZO mantle components in the plume source. Significantly, the observed variance in the geochemistry of Juan Fernandez lavas is consistent with the temporal evolution of Juan Fernandez volcanoes, which sample a heterogeneous plume to a certain extent, as they progress through the pre-shield, shield-building, post-shield, and post-eruptive stages.

In conclusion, results of the combined major-trace element and Sr-Nd-Pb investigation suggest a mantle plume source for the high-$^3He/^4He$ Juan Fernandez OIB and do not support contributions from asthenospheric mantle and/or crustal contamination. Juan Fernandez is unlike other high-$^3He/^4He$ volcanic chains because it does not display mixing between its two mantle plume (EM-1 and FOZO) components and, thus, does not have the commonly observed correlation between He and Sr-Nd-Pb isotopic ratios in other high-$^3He/^4He$ OIB. The true origin of the high-$^3He/^4He$ OIB can be better constrained in the future through more extensive sampling and complementary detailed volatile studies.

# References


Allègre, C. J., and J. F. Minster, Quantitative models of trace element behavior in magmatic processes, *Earth and Planetary Science Letters*, *38*, 1–25, 1978.

Allègre, C. J., S. R. Hart, and J. F. Minster, Chemical structure and evolution of the mantle and continents determined by inversion of Nd and Sr isotopic data, II, Numerical experiments and discussion, *Earth and Planetary Science Letters*, *66*, 191–213, 1983.

Baker, P. E., A. Gledhill, P. K. Harvey, and C. J. Hawkesworth, Geochemical evolution of the Juan Fernandez Islands, SE Pacific, *Journal of the Geological Society*, *144*, 933–944, 1987.

Booker, J., E. C. Bullard, and R. L. Grasty, Palaeomagnetism and age of rocks from Easter Island and Juan Fernandez, *Geophysical Journal International*, *12*, 469–471, 1967.

Castillo, P. R., The recycling of marine carbonates and sources of HIMU and FOZO ocean island basalts, *Lithos*, *216*, 254–263, 2015.

Castillo, P. R., P. Scarsi, and H. Craig, He, Sr, Nd, and Pb isotopic constraints on the origin of the Marquesas and other linear volcanic chains, *Chemical geology*, *240*, 205–221, 2007.

Castillo, P. R., D. A. Clague, A. S. Davis, and P. F. Lonsdale, Petrogenesis of Davidson Seamount lavas and its implications for fossil spreading center and intraplate magmatism in the eastern Pacific, *Geochemistry Geophysics Geosystems*, *11*, Q02,005, 2010.

Chauvel, C., A. W. Hofmann, and P. Vidal, HIMU-EM: the French Polynesian connection, *Earth and Planetary Science Letters*, *110*, 99–119, 1992.

Chauvel, C., R. C. Maury, S. Blais, E. Lewin, H. Guillou, G. Guille, P. Rossi, and M.-A. Gutscher, The size of plume heterogeneities constrained by Marquesas isotopic stripes, *Geochemistry, Geophysics, Geosystems*, *13*, Q07,005, 2012.

Cheng, Q. C., J. D. Macdougall, and P. Zhu, Isotopic constraints on the Easter Seamount Chain source, *Contributions to Mineralogy and Petrology*, *135*, 225–233, 1999.

Corvalan, J., Plate Tectonic Map of the Circum-Pacific Region, Southeast Quadrant, 1981.

Craig, H., and J. E. Lupton, Helium-3 and mantle volatiles in the ocean and the oceanic crust, *The Sea (Emiliani, C., ed.)*, *7*, 391–428, 1981.

Devey, C., C. Hémond, and P. Stoffers, Metasomatic reactions between carbonated plume melts and mantle harzburgite: the evidence from Friday and Domingo Seamounts (Juan Fernandez chain, SE Pacific), *Contributions to Mineralogy and Petrology*, *139*, 68–84, 2000.

Eiler, J. M., K. A. Farley, J. W. Valley, E. Hauri, H. Craig, S. R. Hart, and E. M. Stolper, Oxygen isotope variations in ocean island basalt phenocrysts, *Geochimica et Cosmochimica Acta*, *61*, 2281–2293, 1997.

Farley, K. A., Rare Gases and Radiogenic Isotopes in South Pacific Ocean Island Basalts, Ph.D. thesis, University of California, San Diego., 1991.

Farley, K. A., J. H. Natland, and H. Craig, Binary mixing of enriched and undegassed (primitive?) mantle components (He, Sr, Nd, Pb) in Samoan lavas, *Earth and Planetary Science Letters*, *111*, 183–199, 1992.

Farley, K. A., A. Basu, and H. Craig, He, Sr and Nd isotopic variations in lavas from the Juan-Fernandez Archipelago, SE Pacific, *Contributions to Mineralogy and Petrology*, *115*, 75–87, 1993.

Feigenson, M. D., A. W. Hofmann, and F. J. Spera, Case studies on the origin of basalt, *Contributions to mineralogy and petrology*, *84*, 390–405, 1983.

Foulger, G. R., *Plates vs. plumes: a geological controversy.*, John Wiley & Sons, 2011.

Frey, F. A., The origin of pyroxenites and garnet pyroxenites from Salt Lake Crater, Oahu, Hawaii: trace element evidence, *Am. J. Sci*, *280*, 427–449, 1980.

Garapić, G., M. G. Jackson, E. H. Hauri, S. R. Hart, K. A. Farley, J. S. Blusztajn, and J. D. Woodhead, A radiogenic isotopic (He-Sr-Nd-Pb-Os) study of lavas from the Pitcairn hotspot: Implications for the origin of EM-1 (enriched mantle 1), *Lithos*, *228229*, 1 – 11, 2015.

Gast, P. W., G. R. Tilton, and C. Hedge, Isotopic composition of lead and strontium from Ascension and Gough islands, *Science*, *145*, 1181–1185, 1964.

Gautheron, C., and M. Moreira, Helium signature of the subcontinental lithospheric mantle, *Earth and Planetary Science Letters*, *199*, 39–47, 2002.

Gerlach, D. C., S. R. Hart, V. W. J. Morales, and C. Palacios, Mantle heterogeneity beneath the Nazca plate: San Felix and Juan Fernandez islands, *Nature*, *322*, 165–169, 1986.

Graham, D., W. Jenkins, M. Kurz, and R. Batiza, Helium isotope disequilibrium and geochronology of glassy submarine basalts, *Nature*, *326*, 384–386, 1987.

Graham, D. W., Noble gas isotope geochemistry of mid-ocean ridge and ocean island basalts: Characterization of mantle source reservoirs, *Reviews in Mineralogy and Geochemistry*, *47*, 247–317, 2002.

Graham, D. W., A. Zindler, M. D. Kurz, W. J. Jenkins, and R. Batiza, He, Pb, Sr and Nd isotope constraints on magma genesis and mantle heterogeneity beneath young Pacific seamounts, *Contributions to Miner*, *99*, 446–463, 1988.

Gripp, A. E., and R. G. Gordon, Young tracks of hotspots and current plate velocities, *Geophysical Journal International*, *150*, 321–361, 2002.

Hanan, B. B., and D. W. Graham, Lead and Helium Isotope Evidence from Oceanic Basalts for a Common Deep Source of Mantle Plumes, *Science*, *272*, 991–995, 1996.

Hart, S. R., E. H. Hauri, L. A. Oschmann, and J. A. Whitehead, Mantle Plumes and Entrainment: Isotopic Evidence, *Science*, *256*, 517–520, 1992.

Hilton, D., G. G. Macpherson, and T. R. Elliott, Helium isotope ratios in mafic phenocrysts and geothermal fluids from La Palma, the Canary Islands (Spain): implications for HIMU mantle sources, *Geochimica et Cosmochimica Acta*, *64*, 2119–2132, 2000.

Hilton, D. R., G. M. McMurtry, and R. Kreulen, Evidence for extensive degassing of the Hawaiian Mantle Plume from helium-carbon relationships at Kilauea Volcano, *Geophysical Research Letters*, *24*, 3065–3068, 1997.

Hilton, D. R., K. Gronvold, C. G. Macpherson, and P. R. Castillo, Extreme $^{3}He/^{4}He$ ratios in northwest Iceland: constraining the common component in mantle plumes, *Earth and Planetary Science Letters*, *173*, 53–60, 1999.

Hoernle, K., W. Reinhard, J. P. Morgan, D. Garbe-Schönberg, J. Bryce, and J. Mrazek, Existence of complex spatial zonation in the Galápagos plume, *Geology*, *28*, 435–438, 2000.

Hofmann, A. W., Mantle geochemistry: the message from oceanic volcanism, *Nature*, *385*, 219–229, 1997.

Hofmann, A. W., Sampling Mantle Heterogeneity through Oceanic Basalts: Isotopes and Trace Elements, *Treatise in Geochemistry*, *2*, 61101, 2003.

Hofmann, A. W., and W. M. White, Mantle plumes from ancient oceanic crust, *Earth and Planetary Science Letters*, *57*, 421–436, 1982.

Honda, M., and J. D. Woodhead, A primordial solar-neon enriched component in the source of EM-I-type ocean island basalts from the Pitcairn Seamounts, Polynesia, *Earth and Planetary Science Letters*, *236*, 597–612, 2005.

Jackson, M. G., M. D. Kurz, S. R. Hart, and R. K. Workman, New Samoan lavas from Ofu Island reveal a hemispherically heterogeneous high $^3$He/$^4$He mantle, *Earth and Planetary Science Letters*, *264.3-4*, 360–374, 2007.

Jackson, M. G., S. R. Hart, A. E. Saal, N. Shimizu, M. D. Kurz, J. S. Blusztajn, and A. C. Skovgaard, Globally elevated titanium, tantalum, and niobium (TITAN) in ocean island basalts with high $^3$He/$^4$He, *Geochemistry Geophysics Geosystems*, *9.4*, 21, 2008.

Janney, P. E., and P. R. Castillo, Basalts from the Central Pacific Basin: Evidence for the origin of Cretaceous igneous complexes in the Jurassic western pacific, *Journal of Geophysical Research: Solid Earth*, *101*, 2875–2893, 1996.

Johnson, K. T. M., Experimental determination of partition coefficients for rare earth and high-field-strength elements between clinopyroxene, garnet, and basaltic melt at high pressures, *Contributions to Mineralogy and Petrology*, *133*, 60–68, 1998.

Kay, R., N. J. Hubbard, and P. W. Gast, Chemical characteristics and origin of oceanic ridge volcanic rocks, *Journal of Geophysical Research*, *75*, 1585–1613, 1970.

Klein, E. M., and C. H. Langmuir, Global correlations of ocean ridge basalt chemistry with axial depth and crustal thickness, *Journal of Geophysical Research: Solid Earth*, *92*, 8089–8115, 1987.

Konter, J. G., H. Staudigel, J. Blichert-Toft, B. B. Hanan, M. Polvé, G. Davies, N. Shimizu, and P. Schiffman, Geochemical stages at Jasper Seamount and the origin of intraplate volcanoes, *Geochemistry, Geophysics, Geosystems*, *Q02001*, 2009.

Kurz, M. D., W. J. Jenkins, and S. R. Hart, Helium isotopic systematics of oceanic islands and mantle heterogeneity, *Nature*, *297*, 43–47, 1982.

Kurz, M. D., W. J. Jenkins, S. R. Hart, and D. Clague, Helium isotopic variations in volcanic rocks from Loihi Seamount and the Island of Hawaii, *Earth and Planetary Science Letters*, *66*, 388–406, 1983.

McDonough, W. F., Partial melting of subducted oceanic crust and isolation of its residual eclogitic lithology, *Philosophical Transactions of the Royal Society of London A: Mathematical, Physical and Engineering Sciences*, *335*, 407–418, 1991.

Minster, J. F., and C. J. Allègre, Systematic use of trace elements in igneous processes, *Contributions to Mineralogy and Petrology*, *68*, 37–52, 1978.

Morgan, W. J., Deep mantle convection plumes and plate motions, *American Association of Petroleum Geologists Bulletin*, *56*, 203–213, 1972.

Natland, J. H., Capture of Helium and Other Volatiles during the Growth of Olivine Phenocrysts in Picritic Basalts from the Juan Fernandez Islands, *Journal of Petrology*, *44*, 421–456, 2003.

Peters, B. J., and J. M. D. Day, Assessment of relative Ti, Ta, and Nb (TITAN) enrichments in ocean island basalts, *Geochemistry, Geophysics, Geosystems*, *15*, 4424–4444, 2014.

Rollinson, H. R., *Using Geochemical Data: Evaluation, Presentation, Interpretation (Longman Geochemistry Series).*, Benjamin Cummings, 1993.

Shaw, D. M., Trace element fractionation during anatexis, *Geochimica et Cosmochimica Acta*, *34*, 237–243, 1970.

Silva, I. G., D. Weis, J. Scoates, and J. Barling, The Ninetyeast Ridge and its relation to the Kerguelen, Amsterdam and St. Paul hotspots in the Indian Ocean, *Journal of Petrology*, p. egt009, 2013.

Sims, K. W., and S. R. Hart, Comparison of Th, Sr, Nd and Pb isotopes in oceanic basalts: Implications for mantle heterogeneity and magma genesis, *Earth and Planetary Science Letters*, *245*, 743–761, 2006.

Sobolev, A. V., A. W. Hofmann, and I. K. Nikogosian, Recycled oceanic crust observed in ghost plagioclasewithin the source of Mauna Loa lavas, *Nature*, *404*, 986–990, 2000.

Stracke, A., A. W. Hofmann, and S. R. Hart, FOZO, HIMU, and the rest of the mantle zoo, *Geochemistry, Geophysics, Geosystems*, *6*, Q05,007, 2005.

Stuart, F. M., S. Lass-Evans, J. G. Fitton, and R. M. Ellam, High $^{3}He/^{4}He$ ratios in picritic basalts from Baffin Island and the role of a mixed reservoir in mantle plumes, *Nature*, *424*, 57–59, 2003.

Sun, S.-S., and W. F. McDonough, Chemical and isotopic systematics of oceanic basalts: implications for mantle comopsition and processes., *In: Saunders, A.D., Norry, M.J. (Eds.), Magmatism in ocean basins. Special Publications, vol. 42. Geological Society, London*, *42*, 313–345, 1989.

Thirlwall, M. F., Pb isotopic and elemental evidence for OIB derivation from young HIMU mantle, *Chemical Geology*, *139*, 51–74, 1997.

Tian, L., P. R. Castillo, P. F. Lonsdale, D. Hahm, and D. R. Hilton, Petrology and Sr-Nd-Pb-He isotope geochemistry of postspreading lavas on fossil spreading axes off Baja California Sur, Mexico, *Geochemistry Geophysics Geosystems*, *12*, Q0AC10, 2011.

Weis, D., M. O. Garcia, J. M. Rhodes, M. Jellinek, and J. S. Scoates, Role of the deep mantle in generating the compositional asymmetry of the Hawaiian mantle plume, *Nature Geoscience*, *4*, 831–838, 2011.

White, W. M., Oceanic Island Basalts and Mantle Plumes: The Geochemical Perspective, *Annual Review of Earth and Planetary Sciences*, *38*, 133–160, 2010.

White, W. M., and R. A. Duncan, Geochemistry and geochronology of the Society Islands: New evidence for deep mantle recycling, *Geophysical Monograph Series*, *95*, 183–206, 1996.

Wilson, J. T., A possible origin of the Hawaiian Islands, *Canadian Journal of Physics*, *41*, 863–870, 1963.

Zindler, A., and S. R. Hart, Chemical Geodynamics, *Annual Review of Earth and Planetary Sciences*, *14*, 493–571, 1986.

Zindler, A., H. Staudigel, and R. Batiza, Isotope and trace element geochemistry of young Pacific seamounts: Implications for the scale of upper mantle heterogeneity, *Earth Planetary Science Letters*, *70*, 175–195, 1984.